Atmos. Chem. Phys. Discuss., 12, 32515–32564, 2012
www.atmos-chem-phys-discuss.net/12/32515/2012/
doi:10.5194/acpd-12-32515-2012

Atmospheric Chemistry and Physics Discussions

Dynamics of nitrogen oxides and ozone above and within a mixed hardwood forest in Northern Michigan

B. Seok[1,2], D. Helmig[1], L. Ganzeveld[3], M. W. Williams[1,4], and C. S. Vogel[5]

[1]Institute of Arctic and Alpine Research, University of Colorado, Boulder, CO, USA
[2]Department of Atmospheric and Oceanic Sciences, University of Colorado, Boulder, CO, USA
[3]Department of Environmental Sciences, Wageningen University and Research centre, Wageningen, The Netherlands
[4]Department of Geography, University of Colorado, Boulder, CO, USA
[5]University of Michigan Biological Station, University of Michigan, Pellston, MI, USA

Received: 21 November 2012 – Accepted: 21 Novermber 2012 – Published: 18 December 2012

Correspondence to: D. Helmig (detlev.helmig@colorado.edu) and B. Seok (seok@colorado.edu)

Published by Copernicus Publications on behalf of the European Geosciences Union.

Abstract

The dynamic behavior of nitrogen oxides (NO_x=NO + NO_2) and ozone (O_3) above and within the canopy at the University of Michigan Biological Station AmeriFlux (UMBS Flux) site was investigated by continuous multi-height vertical gradient measurements during the summer and the fall of 2008. A daily maximum in nitric oxide (NO) levels was consistently observed during the morning hours between 06:00 and 09:00 EST above the canopy. Daily NO maxima ranged between 0.2 and 2 ppbv (with a median of 0.3 ppbv), which was 2 to 20 times above its atmospheric background. The sources and causes of this NO maximum were evaluated using NO_x and O_3 measurements and synoptic and micrometeorological data. This analysis was further supported by numerical simulations with a multi-layer canopy exchange model implemented into a single-column chemistry-climate model. The observations indicated that the morning NO maximum was caused by the photolysis of NO_2 from non-local air masses, which were transported into the canopy from aloft during the morning breakup of the nocturnal boundary layer. The analysis of simulated process tendencies indicated that the downward turbulent transport of NO_x into the canopy compensates for the removal of NO_x through chemistry and dry deposition. The sensitivity of NO_x and O_3 concentrations on soil and foliage NO_x emissions was also assessed with the model. Uncertainties associated with the emissions of NO_x from the soil or from leaf-surface nitrate photolysis did not explain the observed diurnal behavior in NO_x (and O_3), and in particular, the morning NO_x peak mixing ratio. However, when considering the existence of a NO_2 compensation point, an increase in the early morning NO_x and NO peak mixing ratios by ~ 30 % was simulated. This increase suggests the potential importance of leaf-level, bi-directional exchange of NO_2 in understanding the observed temporal variability in NO_x at UMBS.

ACPD

12, 32515–32564, 2012

1 Introduction

Nitrogen oxides (NO_x=NO + NO_2), which originate from soil emissions, lightning, and combustion, play a critical role in regulating the photochemical production of ozone (O_3) in the troposphere (Crutzen, 1970; Jacob, 2000; Crutzen and Lelieveld, 2001; Hauglustaine et al., 2001). Excessive deposition of NO_x, which contributes to the total nitrogen input on ecosystems, and exposure of vegetation to toxic levels of O_3 can cause foliage damage; these are linked to acidification and eutrophication of forests (Mosier et al., 2001; Grunhage et al., 2002).

NO_x and O_3 concentrations (and fluxes) have been measured in forest ecosystems to quantify NO_x and O_3 dry deposition in relatively polluted conditions (e.g. CASTNET; US Environmental Protection Agency, 2009). Other measurements of NO_x and O_3 were done to study the role of canopy interactions between biogenic emissions, dry deposition, chemistry, and turbulence in determining bidirectional exchange of NO_x between more pristine forests and the overlying atmosphere (e.g. Bakwin et al., 1990, 1994; Carroll and Thompson, 1995; Munger et al., 1996; Rummel et al., 2002). The University of Michigan Biological Station (UMBS) is one of those sites, with a history of NO_x and O_3 measurements since 1997 from the Program for Research on Oxidants: PHotochemistry, Emissions and Transport (PROPHET; Carroll et al., 2001). At the PROPHET site, Thornberry et al. (2001) observed a periodic mixing ratio maximum of NO_x in the morning hours above the forest canopy. A similar behavior was also observed at other forest sites (e.g. Parrish et al., 1993; Munger et al., 1996; Andreae et al., 2002; Farmer and Cohen, 2008). Alaghmand et al. (2011) concluded that to understand the diurnal behavior in NO_x mixing ratios at sites such as UMBS, the combined role of (nocturnal) mixing and transport processes needs to be considered and this would require the coupling of canopy and boundary layer turbulence models.

In this study, we used the combined analysis of below, within, and above canopy observations and model simulations (1) to investigate the cause for the observed morning peak mixing ratios of NO_x and (2) to assess the sensitivity of in-canopy NO_x (and O_3)

ACPD
12, 32515–32564, 2012

to potentially relevant in-canopy sources and sinks under atmospheric conditions encountered at UMBS. Results are based on an analysis of a 5-month data set of NO_x, NO, and O_3 vertical mixing ratio profiles, which were measured above and within the canopy of the UMBS forest in the summer and the fall of 2008. The analysis was supported by simulations with a multi-layer canopy-boundary layer exchange model.

2 Measurements

2.1 Site description

This study was conducted from 19 July to 21 November 2008 at the AmeriFlux site in the UMBS domain (45.5932° N, 84.7130° W; Schmid et al., 2003). This site is located in an area rather distant from major anthropogenic sources although it is quite often (~ 40 % of the time) affected by advection of polluted air masses. The nearest metropolitan areas (population > 200 000) are Detroit, Michigan, ~ 350 km to the southeast; Milwaukee, Wisconsin, ~ 350 km to the southwest; and Chicago, Illinois, ~ 450 km also to the southwest.

The UMBS forest falls in the transition zone between mixed hardwood and boreal forests with a mean annual (from 1979 to 2009) temperature of 6.7 °C and rainfall of 803.4 mm (Vande Kopple, 2011). The pre-settlement forest, dominated by white pine (*Pinus strobus*), red pine (*Pinus resinosa*), and hemlock (*Tsuga canadensis*), was cut around 1880. The area was disturbed repeatedly by fire until 1923. Today, within a 1 km radius of the AmeriFlux tower, the forest is composed mainly of bigtooth aspen (*Populus grandidentata*) and trembling aspen (*Populus tremuloides*), but there is also significant representation of maple (*Acer rubrum*), red oak (*Quercus rubra*), birch (*Betula papyrifera*), and beech (*Fagus grandifolia*). In patches, there is a dense understory of young white pine, up to ~ 6 m high. The understory layer near the forest floor is dominated by bracken fern (*Pteridium aquilinum*) and saplings of red maple, red oak, beech, and white pine (Gough et al., 2007).

ACPD
12, 32515–32564, 2012

The forest at UMBS has two distinctive layers: a crown layer and an understory layer (Fig. 1). The mean canopy height around the AmeriFlux tower is ~ 22 m (Schmid et al., 2003). The average seasonal maximum (from 1999 to 2009) of the cumulative single-sided leaf area index (LAI, $m^2\,m^{-2}$) is 3.5. The average seasonal LAI began to decrease in early-October, and it reached its average seasonal minimum of 1.5 by November.

2.2 Instrumentation

A UV absorbance monitor (DASIBI 1003-AH) was used to measure the mixing ratio of O_3 through the canopy. Before installing the DASIBI at the site, a 5-point calibration was conducted against a TEI 49C monitor (Thermo Electron Corporation (TECO), Franklin, MA), which served as the transfer standard for the calibration. Brodin et al. (2010) describe the calibration of this transfer standard in detail. The calibration of the DASIBI resulted in a 1 ppbv offset with a 3 % slope correction. The O_3 data from the DASIBI were corrected for this difference. The detection limit of the DASIBI was 1 ppbv.

The mixing ratio of NO_x was determined with a chemiluminescence analyzer (TEI 42C-TL; TECO). This instrument follows the Federal Reference Method as designated by the US EPA, which is also the most prevalent method of measuring ambient air NO_x (Demerjian, 2000). The TEI 42C-TL had two channels. The first channel measured nitric oxide (NO) via $NO + O_3$ chemiluminescence. The second channel measured nitrogen dioxide (NO_2) by redirecting air through a heated (325 °C) molybdenum converter, which caused NO_2 – including other oxidized nitrogen compounds – to be converted to NO. The NO_2 mixing ratio was then determined by subtracting NO, measured in the first channel. There were several interferences in this NO_2 measurement scheme (Steinbacher et al., 2007). The error in the NO_2 measurement increased with rising levels of interfering gases such as nitrous acid (HONO), peroxyacetyl nitrate (PAN), and alkyl nitrates that contributed to the NO_2-mode signal. However, in urban environments, NO_x typically constituted the largest fraction of oxidized nitrogen compounds (Spicer, 1982; Steinbacher et al., 2007); hence, NO_2 mixing ratios obtained with the TEI 42C-TL would represent a reasonable estimate if the site was influenced

ACPD
12, 32515–32564, 2012

by anthropogenic sources. Before the deployment of the TEI 42C-TL analyzer in the summer of 2008, the instrument was sent to TECO for preventive maintenance. TECO reported the instrument to have a NO_2 conversion efficiency of 99.9 % after servicing it. Ultra-zero air (Airgas Great Lakes, Inc., Royal Oak, MI) was used to establish baseline conditions and for dilution of a NIST-traceable 1 ppmv NO gas standard (Scott-Marrin, Inc., Riverside, CA) to 0.5 ppbv and 10 ppbv calibration gas levels. After propagating the uncertainties of the mass flow controllers and the NO gas standard, we estimated the instrument to have a 5 % accuracy error. The signal noise was 0.05 ppbv, which resulted in a detection limit of ~ 0.1 ppbv.

2.3 Sampling

Vertical mixing ratio profiles of NO_x and O_3 were measured from the AmeriFlux tower at 4, 15, 21, 25, 34, and 40 m above the ground (Fig. 1). Sampling through each inlet was done sequentially from the 40 m height down to the 4 m height. The sampling inlet at a particular height was selected through a manifold constructed of an array of six two-way solenoid valves with polytetrafluoroethylene (PTFE) body seals (Norgren USA, Littleton, CO). Each sampling interval was 5 min long with gas mixing ratios being determined in this flow every minute. A complete cycle took 30 min, thus there were 48 cycles per day.

Perfluoroalkoxy (PFA) inlet funnels with 1 mm grids (Savillex Co., Minnetonka, MN) were used to prevent large debris from being drawn into the sampling line. Single stage 47 mm PFA filter clamps (Savillex Co.) with 5 mm PTFE membrane filter (Millipore Co., Bellerica, MA) were placed upstream of the instrument inlet to prevent fine particles from interfering with NO_x and O_3 measurements.

All sampling lines, valves, and filters were conditioned for three days with a flow of 2 L min^{-1} of air containing 200 ppbv of O_3 prior to installation. This was done to minimize the loss of O_3 in the manifold during subsequent field sampling. Six equal-length 61 m-long PFA Teflon® tubes with outer diameter of 6.4 mm and inner diameter of 3.6 mm (Parker Hannifin, Cleveland, OH) were used as sampling lines. The excess

ACPD
12, 32515–32564, 2012

tubing for the sampling inlets closer to the instruments were coiled and kept in the same housing unit as the instruments.

The flow rate through the DASIBI was 1.8 L min^{-1}, and the TEI 42C-TL flow rate was 1.2 L min^{-1}. Therefore, the total flow rate through each sampling line was 3 L min^{-1}. The theoretical transport time of air samples from the inlet to the gas analyzers was calculated (using tubing dimensions, manifold volume, and purge rate) to be 15 s.

2.3.1 Bias in the sampling lines

All the sampling inlets were intercompared by bringing them to the 15 m height of the tower. This was done to determine the potential measurement bias, as there are inherent differences in the sampling lines. Mixing ratios of NO and O_3 and line pressure were monitored through each line over a 2-day period. The sampling lines varied < 0.1 ppbv in NO, < 1 ppbv in O_3, and < 2 kPa in pressure against each other.

2.3.2 Correcting for the loss of NO in the sampling lines

NO undergoes rapid oxidation through its reaction with O_3 and other free radicals, e.g. hydroperoxy (HO_2) and alkylperoxy (RO_2), in the atmosphere. Therefore, it is necessary to correct for the loss of NO during the transport in the sampling line to the analyzer. Since ambient air HO_2 and RO_2 levels are two to three orders of magnitude smaller than NO (Fuchs et al., 2008), it was assumed they would not affect the sampled NO mixing ratios. The loss of NO due to oxidation by O_3 alone was considered in the correction. In the absence of light, NO is oxidized to NO_2 by

$$NO + O_3 \xrightarrow{k} NO_2 + O_2 \qquad \text{(R1)}$$

where k is the reaction rate constant ($k = 1.4 \times 10^{-12} e^{-1310/T}$ [cm^3 molecules^{-1} s^{-1}], for T between 195 and 308 K; Atkinson et al., 2004).

The reaction rate constants were calculated using ambient temperature recorded when the air sample was collected. The conversion rate of NO was then determined

ACPD
12, 32515–32564, 2012

from (R1) using the O_3 mixing ratio measured at any given moment from the same inlet. From this conversion rate, the percentage of NO lost after 15 s, which was the residence time of the air sample in the tube, was calculated. Up to 32 % of the NO was converted to NO_2 by O_3, depending on the air sample temperature, O_3 mixing ratio, and line pressure. The NO mixing ratio was corrected for this loss. NO_2 mixing ratios were recalculated accordingly by subtracting the correct NO mixing ratio from the 42C-TL's output of the NO_x mixing ratio.

2.4 Ancillary data

Meteorological instrumentation on the AmeriFlux tower provided the ancillary data used in the analyses (see Schmid et al., 2003, for information about the instruments). Wind speed, wind direction, turbulence, and incoming solar radiation were measured from the 46 m height of the tower (Fig. 1). Turbulence data (u' and w'), measured from the 3-D sonic anemometer, were used to calculate the friction velocity ($u_* = -\langle u'\,w'\rangle^{0.5}$ [$\mathrm{m\,s^{-1}}$]) above the canopy. Temperatures below and above the canopy were measured from temperature sensors at 4, 21, 34, and 46 m on the tower (Fig. 1). From the temperature data, temperature lapse rates ($\gamma = \left(T_{z_1} - T_{z_2}\right) / (z_1 - z_2)$) through the canopy (4 and 21 m) and above the canopy (21 and 34 m) were calculated to diagnose stability.

3 Single column canopy model

3.1 Model description and initialization parameters

A multi-layer atmospheric-biosphere exchange model implemented in a single column chemistry-climate model (SCM; Ganzeveld et al., 2002a, 2006, 2008) was used to evaluate the dynamical behavior of NO_x and O_3 mixing ratios observed above and within the forest canopy. In contrast to most site-scale atmosphere-biosphere exchange models, the SCM does not use observed meteorological parameters to simulate exchanges.

ACPD
12, 32515–32564, 2012

Instead, the SCM determines the dynamic behavior of the system (including the hydrological cycle, boundary layer dynamics, convection, and cloud formation) from initial vertical profiles and surface properties online and reanalysis of weather data (see below).

The atmosphere-biosphere trace gas exchange calculations in the SCM included dry deposition, biogenic emissions, in-canopy chemical transformations, turbulence, and the extinction of radiation within the canopy. All processes were simulated explicitly as a function of the SCM's meteorological, hydrological, and atmospheric chemistry parameters as well as the canopy structure distinguishing a crown layer and an understory layer. Stomatal and non-stomatal removal in the dry deposition of NO_x and O_3 (and other gases) is considered in the SCM. The stomatal conductance is calculated from in-canopy radiation profiles and soil moisture status, whereas the non-stomatal removal is a function of cuticular and soil uptake resistances (Ganzeveld and Lelieveld, 1995). The soil biogenic NO emission flux is normally calculated by the SCM according to a modified implementation of the Yienger and Levy (1995) algorithm. However in this study, a range of constant soil NO emission fluxes was applied in a sensitivity analysis with the reference soil NO emission flux being selected based on the observed emission flux of soil NO at the site (see Sect. 5.2.1). The model also considers the potentially relevant contribution to canopy NO_x by photolysis of nitrate that has accumulated on the leaf surface (e.g. Zhou et al., 2003). The emissions of biogenic volatile organic compounds (BVOCs; i.e. isoprene and monoterpenes) are calculated in the SCM according to Guenther et al. (1995) or alternatively with the Model of Emission of Gases and Aerosols from Nature (MEGAN; Guenther et al., 2006). In this study, we applied the Guenther et al. (1995) implementation based on observed emission factors at the leaf-scale reported for this site (Ortega et al., 2007, see Table 1). This results in a simulated canopy isoprene emission flux comparable to that reported by Pressely et al. (2005).

The atmosphere-biosphere exchange simulations also require initialization of a selection of biogeophysical parameters, e.g. LAI, canopy height, surface roughness, and

ACPD
12, 32515–32564, 2012

the vertical distribution of biomass (expressed by the leaf area density profile). Values used for these parameters to simulate conditions found at UMBS are also provided in Table 1 (and in Fig. 1 for the leaf area density profile).

A key feature of the SCM for site-scale evaluation is the consideration of advection and synoptic weather systems. To consider changes in weather, reanalysis data from the European Centre for Medium range Weather Forecast (ECMWF) were applied, which typically results in realistic representation of the site meteorology (Ganzeveld et al., 2006). For the representation of advection of long-lived trace gases, the simulated boundary layer mixing ratios above the canopy (but not those inside and below the canopy) of NO_x and O_3 in the SCM were "nudged" (forced) towards observed mixing ratios. In this study, our tracer nudging used a relaxation time of 300 s (for a model time step of 60 s) to capture some of the rapid fluctuations in the observed mixing ratios while avoiding numerical instabilities.

3.2 Model run scenarios

Three sets of model runs were performed to evaluate the role of the "biogenic" versus the "anthropogenic" exchange regime in explaining the observed diurnal variability in NO_x and O_3 at UMBS. All the model runs simulated the month of August observations. Two different model runs focused on the sensitivity to soil NO emissions and on foliage NO_x emissions by varying the emission rates by 0, 1, 10, and 25 times the default values (see Table 1). One other additional simulation focused on the role of leaf-scale bidirectional NO_x exchanges.

4 Results and discussion of observations

4.1 Meteorological data

We focus our analysis on observations for the months of August and November. These two months were selected since August represented a state of the forest canopy during

ACPD
12, 32515–32564, 2012

a period of highest mean seasonal LAI. In contrast, November was chosen as a period after leaf abscission when the forest canopy was at its lowest mean seasonal LAI.

Weather conditions between July and November in 2008 were typical for UMBS. Temperature variations at UMBS were within the ranges of the temperature normal from 1979 to 2010, but total precipitation during this period was lower than the average climatic conditions. This deviation in total precipitation was not considered anomalous or extreme as they were within 1-standard deviation from the mean (Table 2).

Figure 2 shows the seasonal decline in the daily maximum of incoming solar radiation from July to November (i.e. daytime maxima of $\sim 700\,\mathrm{W\,m^{-2}}$ and $\sim 250\,\mathrm{W\,m^{-2}}$, respectively). Similarly, the daily temperature amplitude above canopy decreased from $\sim 11\,^{\circ}\mathrm{C}$ in July to $\sim 4\,^{\circ}\mathrm{C}$ in November. The daily amplitude in friction velocity seem to track the pattern of the incoming solar radiation with decreasing absolute amplitude (difference between daily minimum and daily maximum) over the 5-month period with daytime maxima $> 1\,\mathrm{m\,s^{-1}}$, indicating intense daytime turbulent exchange and minimum nocturnal friction velocities $\sim 0.2\,\mathrm{m\,s^{-1}}$ reflecting the suppressed nighttime mixing conditions.

The monthly average daily cycle of solar radiation, temperature lapse rate, and friction velocity for August and November are shown in Fig. 3. Sunrise shifted from 06:00 to 07:30 EST between August and November. Sunset changed from 19:00 EST in August to 17:30 EST in November. The diurnal pattern of the observed above-canopy friction velocity closely followed the solar radiation cycle. Friction velocity increased from a typical nocturnal minimum of $\sim 0.2\,\mathrm{m\,s^{-1}}$ to a maximum $> 1\,\mathrm{m\,s^{-1}}$, implying efficient turbulent mixing in the above-canopy layer at night. Apparent increases in mixing (or friction velocity) were observed > 30 min after sunrise.

Since no direct turbulence measurements inside the canopy were available, temperature lapse rates from the vertical temperature profile measurements (see Sect. 2.4) were used, in addition to friction velocity, as a proxy for the efficiency of turbulent mixing inside and above the canopy. These layers were considered to be in the stable regime when the temperature lapse rate (for the canopy layer calculated from

ACPD
12, 32515–32564, 2012

observed temperatures at 4 and 21 m and for the above-canopy layer calculated from temperatures observed 21 and 34 m) was below 0.0098 $^{\circ}$C m^{-1}, the dry adiabatic lapse rate (denoted as the dotted line in the lapse rate plots; Fig. 3). The atmosphere was considered unstable when the lapse rate was above the dry adiabatic lapse rate, and it was considered neutral when the lapse rate equaled the dry adiabatic lapse rate. The fact that changes in the above-canopy lapse rate, which reflect a transition from stable to unstable mixing conditions, coincide with the observed fast increase in friction velocity > 30 min after sunrise supports the use of these lapse rates as proxy for mixing conditions.

The daily amplitude (i.e. the difference between daily minimum and maximum) of the lapse rates decreased with a decrease in solar radiation from August to November. This suggests a decreasing role of buoyancy in turbulent exchanges. The timing when atmospheric stability changed varied as a function of the timing of sunrise and sunset implying also a dependence of the stability regime on solar radiation.

In August, stable atmospheric conditions were observed at night prior to sunrise through and above the canopy, indicating suppressed mixing between the two layers. Within 30 min after sunrise (~ 06:30 EST), the lapse rates diverge with enhanced mixing conditions in the above-canopy layer but increasing stability in the canopy layer. This response indicates differential heating of the above-canopy layer and the top of the canopy by the incoming solar radiation. The divergence in the lapse rates also indicates that the layers appear to be decoupled, thus mixing is suppressed resulting in the accumulation of biogenically produced trace gases inside the canopy. As the sun sets (~ 19:00 EST), the temperature lapse rates of the two layers converge to a lapse rate reflecting a stable regime.

In November, the mixing of air mass into the canopy layer was strongly suppressed. The canopy layer remained decoupled from the above-canopy layer throughout the day. The above-canopy layer mixing conditions transitioned from a neutral regime to an unstable regime about 30 min after sunrise (~ 08:00 EST); after sunset (~ 17:30 EST), the

ACPD
12, 32515–32564, 2012

above-canopy layer lapse rate transitioned from unstable to neutral mixing conditions. The canopy layer lapse rate remained stable throughout the day.

4.2 Chemical data

4.2.1 Seasonal data

The evolution of NO_x, NO, and O_3 canopy mixing ratio profiles is shown in Fig. 2. Gaps in the data were due to taking the instrument offline for calibrations and repairs and due to intercomparison tests of the sampling lines. The gap in chemical data below the canopy from 27 September onward was due to failures in the solenoid switching valves.

Daily amplitudes of NO_x, NO, and O_3 gradually decreased over the season. For instance, the daily amplitude in NO_x mixing ratios averaged at 1 ppbv in August, then it declined to 0.5 ppbv in November. However, the daily NO_x maximum increased with time. The daily NO_x maxima in August ranged between 0.4 and 10 ppbv with a median of 2 ppbv. For NO, its daily amplitude averaged at 0.3 ppbv in August, and then it declined to 0.2 ppbv in November. The daily NO maximum in August ranged between 0.2 and 2 ppbv with a median of 0.3 ppbv. O_3 varied daily by an average of 20 ppbv in August; the daily amplitude declined to 5 ppbv in November. Its daily maximum ranged between 16 and 66 ppbv with a median of 33 ppbv. These wide ranges in maximum NO_x and O_3 mixing ratios reflect that this site is influenced by contrasting biogenic and anthropogenic footprints, which may be dependent on season (Cooper et al., 2001).

4.2.2 Diurnal data

Mean diurnal vertical mixing ratio profiles of NO_x, NO, and O_3 for August and for November are shown in the color contour plots in Fig. 4.

– **NO_x**. The most prominent feature in the diurnal NO_x cycle is the mixing ratio maximum seen during the early morning hours. Elevated NO_x was observed

ACPD
12, 32515–32564, 2012

throughout and above the canopy, with highest mixing ratios occurring right above the canopy. The diurnal cycle of NO_x also shows elevated levels of NO_x throughout the canopy during the night (~ 0.5 to 0.7 ppbv) and lower levels during the latter part of the day (~ 0.3 ppbv). The daily amplitude in NO_x mixing ratio and the magnitude of the morning peak are smaller in November than in August. The differences in the nocturnal NO_x mixing ratios between August and November are small.

– **NO**. The diurnal variation of NO also clearly shows a morning peak above the canopy after sunrise, coinciding with the morning NO_x maximum. This coincidence in timing of the NO peak suggests that this NO is formed from NO_2 photodissociation. During the night, despite the previously discussed canopy stratification, observed understory layer NO levels are slightly (< 0.1 ppbv) larger than the above-canopy layer NO levels, which indicates that soil NO emission may have minor influence on the nocturnal NO profile.

– **O_3**. Ozone increased throughout the daylight hours reaching maxima in the early afternoon. Mixing ratios then began leveling out in the late afternoon and began dropping steadily throughout the evening and night until approximately sunrise time. In the understory layer ozone declined at a faster rate, with ozone loss first occurring right at the forest ground surface, and then from there slowly reaching up to the crown layer. During nighttime ozone mixing ratios above-canopy remained ~ 10 ppbv higher than in the understory. Between 08:00 and 09:00 EST, the O_3 mixing ratio in the understory rapidly increased to levels measured in the above-canopy layer. During the day, from 10:00 to 17:00 EST, the vertical O_3 profile evolved uniformly all throughout below and above the canopy, with average O_3 maxima of ~ 30 ppbv. It is noteworthy that the spatial and temporal evolution of the nighttime O_3 loss near the ground coincided with the nighttime accumulation of NO_x. This behavior suggest that the ozone loss and NO enrichment are controlled by similar processes, i.e. soil emission fluxes (NO) and surface uptake/deposition

ACPD
12, 32515–32564, 2012

(O_3). Similar to the NO_x diurnal cycle, the daily amplitude in the O_3 mixing ratio was smaller in November than in August.

4.2.3 Air mass advection

Figure 5 shows a wind-pollution rose of the measured trace gases for August and for November. The length of the wedge corresponds to the frequency of readings from particular wind sectors, while the color corresponds to the magnitude of the pollutant mixing ratios. These wind-pollution roses show that the two predominant wind direction at UMBS are from the southeast (SE; 112.5°–157.5°, occurs ~ 20 %) and the northwest (NW; 292.5°–315°, occurs ~ 23 %), and somewhat less, from the west. The wind distribution did not change much between August and November.

The O_3-wind rose plots show enhanced O_3 being transported during S–SE winds (112.5°–247.5°), most notably for November. During November, elevated O_3 levels were also observed during southwest (SW) winds. Relative to O_3, NO_x and to a lesser extent, NO, display a more pronounced wind direction dependency, with elevated levels clearly being associated to SE and SW wind directions. During NW winds, NO_x remained < 1 ppbv during most times, whereas SW–SE winds consistently were associated with NO_x > 2 ppbv. There are major urban centers from 350 to 450 km upwind of UMBS in the SE–SW sectors (i.e. Detroit, Milwaukee, and Chicago); these urban areas are likely the source regions for the elevated NO_x transported to the site.

The diurnal breakup of the wind roses (Appendix, Fig. A1) shows that the site experienced a diurnal shifting of transport direction. During August, from midnight to 06:00 EST, wind directions were predominantly from the NW and the SE – and occasionally from the W. Winds then gradually shifted to NW and SW–SE. During sunrise (06:00–09:00 EST hours), wind directions were predominately from the NW and the SW–SE. From the morning hours to after sunset (09:00–21:00 EST hours), the frequency of SW–SE winds declined and the majority of the winds came from the W–NE directions. During the late evening (21:00–24:00 EST hours), the frequency of SE wind directions increased leading back to predominately NW and SE winds.

ACPD
12, 32515–32564, 2012

The diurnal frequency of wind directions in November varied from August in that the S-SE wind directions stayed more frequent throughout the night and day (Fig. A1). However, from sunrise until after sunset (09:00–21:00 EST hours), the S-SE wind direction dominance decreased and the frequency of W-NW wind directions increased. The steady frequency of S-SE wind directions in November may contribute to the smaller daily variation observed for NO_x and O_3 levels than that observed in August, as winds from these directions tend to bring elevated levels of NO_x and O_3 into the region.

The frequency of NO maxima increased during winds from the southerly directions (SW–SE sectors) (06:00–09:00 EST hours for August; 09:00–12:00 EST hours for November). Therefore, wind direction seems to be a key factor in the observed variations in gas mixing ratio. Cooper et al. (2001) and Thornberry et al. (2001) also observed higher levels of NO_x and O_3 during transport from the SW–SE sectors at UMBS. Conversely, they saw lower levels of NO_x and O_3 with NW winds. Back trajectory analysis done by Cooper et al. (2001) and by Alaghmand et al. (2011) showed that air transported to the site during SW–SE winds had passed through the three major urban areas of Detroit, Milwaukee, and Chicago. The lack of NO_x increases during NW winds at night indicates the lack of major local emissions from that wind sector (Thornberry et al., 2001). Consequently, these wind flow analyses support the hypothesis that the NO_x increases seen at UMBS are most likely non-local. The wind-pollution rose and wind rose analyses provide a strong indication that advection plays a major role in the observed morning maxima of NO_x and NO. This will be further substantiated by the sensitivity analysis with the model for this site presented in Sects. 5.2 and 5.4.

4.3 Seasonal shifting of morning NO_x peak

Figure 6 shows the relationship between the time of sunrise and the occurrence of NO_x and NO maxima from July to November for data falling into the 03:00 to 15:00 EST window (Appendix, Fig. A2). The time of sunrise was determined when the radiation sensor registered $> 10\,W\,m^{-2}$ increase from its nighttime reading ($\sim 0.1\,W\,m^{-2}$). The daily sunrise time determinations are not plotted in the figure, but instead the linear

ACPD
12, 32515–32564, 2012

regression line fit through the data is shown. The slope of the regression line indicates that the sunrise time shifted $\sim 0.147\,\mathrm{h\,wk^{-1}}$. The time of the NO_x peak was determined from the occurrence of the maximum NO_x reading at all measurement heights, box-and-whisker plots in Fig. 6 show the statistical distribution of the weekly data. The data in Fig. 6a clearly illustrate that the majority of the daily NO_x maxima measured from each tower inlet level occurred within a few hours after sunrise. A linear regression line through the median values of the weekly distribution plot of the daily NO_x maxima ($y = 0.136x + 7.14$, $r^2 = 0.478$, where y is sunrise time and x is the weekly bin) indicates that the time of the NO_x maximum shifted by ~ 0.136 (standard error ± 0.0355) $\mathrm{h\,wk^{-1}}$, similar to the change in sunrise time. The difference in the y-intercept of the two (sunrise and NO_x maxima) regression lines can be used as an indicator of the delay of the NO_x maximum relative to sunrise; the offset between the two regression analyses yields a result of $\sim 2\,\mathrm{h}$.

Figure 6b shows the relationship between sunrise time and the time of maximum NO. The linear regression through the median weekly NO maxima indicates that the time of NO maximum shifted by ~ 0.159 (standard error ± 0.0321) $\mathrm{h\,wk^{-1}}$. The lag in when the NO maximum occurs after sunrise is $\sim 2.5\,\mathrm{h}$. Notice that this corresponds to a time approximately half an hour after the NO_x maximum time.

This analysis suggests that the sunrise time and the occurrence of the NO_x maximum are closely linked. Consequently, it appears that solar radiation driven processes, such as thermodynamically driven mixing and photochemistry, are the governing processes in the NO_x and NO morning peak occurrence.

5 Model results and discussion

5.1 Model validation and baseline performance

The model was used to simulate the month of August conditions for UMBS. The simulations utilized the input parameters summarized in Table 1. To assess the performance

ACPD
12, 32515–32564, 2012

of the model on simulating the main features of the site-specific micrometeorology and chemical boundary conditions, the results of the simulations were compared against observed incoming solar radiation, above-canopy air temperature at 34 m, above-canopy friction velocity (Fig. 7), and the NO_x and O_3 mixing ratios at 32 m (Fig. 8).

Figure 7 shows that the SCM was able to simulate the diurnal cycle in radiation and temperature quite well as reflected by a strong correlation between measured and simulated parameter values ($r > 0.95$). However, the model underestimated the daytime maximum friction velocity with a too strong decrease in turbulence intensity simulated by the model in the afternoon. The latter seems to be due to a misrepresentation of the stability effect for unstable conditions in the SCM. Good agreement between the simulated and observed friction velocity was produced when soil moisture was reduced in the SCM, however, this resulted in simulated temperatures that were 4 °C warmer than observations.

Figure 8 shows the mean and median diurnal cycles of observed and simulated NO_x and O_3 mixing ratios. The difference between the mean and median of the observed data is largest during the midnight to early morning hours (00:00–06:00 EST). This feature indicates that the influence exerted by occasional events with elevated NO_x is higher during those hours than during the remainder of the day. O_3 shows a similar behavior, but with generally smaller differences between the median and mean mixing ratios. In addition, the difference between the mean and the median mixing ratios reflects the large temporal variability in the observations of air masses that are enhanced in NO_x and O_3 under suppressed mixing conditions.

The simulated diurnal means of NO_x and O_3 in Fig. 8 include the contribution by advection as the model was nudged towards the observed above-canopy NO_x and O_3 mixing ratios. In other words, the simulations reflect the net result of the explicitly resolved sources, sinks, and vertical exchange processes complemented by the implicitly added "advection" term, which considers changes in chemical composition of air advected to the site. Consequently, the simulated diurnal O_3 above-canopy layer mixing ratios (Fig. 8) nearly resemble the observed data as anticipated. In contrast, agreement

ACPD
12, 32515–32564, 2012

between simulated and observed mean NO_x is less. The disagreement is greatest in the early morning hours, where simulated NO_x is ~ 0.3 ppbv smaller compared to the observed peak mixing ratio of ~ 1.5 ppbv. The fact that the model output shows better agreement with the median data suggests that the morning NO_x peak seen in the August mean data reflects the role of some large peak values associated with individual transport events, which are underrepresented by the model. Apparently, these events are not captured by the model for the selected nudging relaxation time of 300 s. This underestimation of the above-canopy layer NO_x peak mixing ratios has obvious consequences for explanation of the observed early morning peak in NO, which we discuss in later sections.

5.2 Sensitivity of the above and within canopy morning NO_x peak

5.2.1 Soil emissions

The sensitivity of NO_x, NO, and O_3 to soil NO emissions is shown in Fig. 9 as the difference between observed and simulated diurnal mixing ratio profiles (Δ = simulated – observed). The soil NO emission rates tested include a "zero" soil NO emissions flux (0×; Fig. 9b), a soil NO emission flux reflecting reported values (0.07 ng N m^{-2} s^{-1}, Table 1) (1×; Fig. 9c), and 10 and 25 times increases of the reported values (10×, 25×; Fig. 9d, e). Note that the 25× case is most likely an unrealistic and extreme case, as it is larger than any observations suggest (Carleton et al., 2003, unpublished), but it was applied here for the purpose of testing the sensitivity of the model. In addition, these simulations on the soil NO_x emission influence did not include any NO_x contribution by foliage emissions. In Fig. 9b–e, a positive delta value implies that the model overestimates measured mixing ratios, while a negative delta value means an underestimation in the simulated mixing ratio.

– **NO_x**. The observed nighttime minimum of NO_x seen in the data (Fig. 9a) near the forest floor points at the role of understory sinks of NO_x, e.g. surface deposition or chemical destruction, of a magnitude larger compared to the soil NO_x source.

ACPD
12, 32515–32564, 2012

The 0× and 1× soil NO emission flux simulations resulted in NO_x profiles that are similar to each other and resemble the observed data. Apparently, NO_x in the crown and above-canopy layers is rather insensitive to the magnitude of the soil NO emission flux. Even the further increases of the NO soil flux (10× and 25×) did not produce noticeable changes to the NO_x profiles, except in the understory layer. For the 1× soil NO_x source, the model predicted NO_x minimum mixing ratios of ∼ 0.3 ppbv in the understory layer in the early night compared to observed understory NO_x levels of ∼ 0.7 ppbv. This suggests that the model NO soil flux that we selected for this study – based on observed soil NO emission fluxes – appears to be too small. The 10× simulation of 0.7 $ng\,N\,m^{-2}\,s^{-1}$ actually results in a better agreement between simulated and observed NO_x inside the canopy. This finding concurs with Alaghmand et al. (2011), who applied a soil NO flux at UMBS of ∼ 180 $nmol\,m^{-2}\,h^{-1}$ (∼ 0.7 $ng\,N\,m^{-2}\,s^{-1}$) in their work. They based this number on the data set obtained by Carleton et al. (2003) that we also used. However, they included values obtained during and after rain events, which shifted the mean soil flux to this substantially larger value. We excluded the rain event values because the rainfall for 2008 during the measurement period was below average. In addition, Nave et al. (2011) reported NO effluxes of ∼ 0.2 $\mu g\,N\,m^{-2}\,h^{-1}$ (or ∼ 0.07 $ng\,N\,m^{-2}\,s^{-1}$) around the AmeriFlux site in the summer of 2008. At sunrise, the model predicted an increase in NO_x mixing ratios throughout the canopy, whereas the observations showed mainly an increase in NO_x above the canopy (Fig. 9a, b). Observed NO_x mixing ratios were as large as 1.5 ppbv, while the model predicted above-canopy maximum NO_x mixing ratios up to ∼ 1 ppbv, even for the 10× soil emission case. The model predicted minimum NO_x mixing ratios in the canopy layer in the late afternoon and evening consistent with the data from 12:00 to 18:00 EST. For the "unreasonably" high 25× soil emission case, the model predicted levels of NO_x near the forest surface about 1 ppbv larger than observed during the night. Yet even with this high soil NO_x flux, there was no improvement in the representation of the above-canopy early morning NO_x peak.

ACPD
12, 32515–32564, 2012

– **NO**. For all soil NO flux scenarios, the daytime NO mixing ratio profiles were slightly overestimated in the canopy layer. The model simulated NO canopy mixing ratios reasonably well for all soil NO emission cases with differences of < 0.05 ppbv. However, the model underestimated the nocturnal NO mixing ratios in the crown and above-canopy layers by > 0.05 ppbv. The 25× soil emission case shows some enhancement in the simulated NO mixing ratios in the understory layer, but the NO increase is only confined to the understory layer, whereas the observations showed nocturnal NO mixing ratios of ~ 0.1 ppbv throughout the canopy. The simulations show a similar above-canopy NO peak as seen in the data. However, the NO maxima simulated by the model are 0.05 to 0.1 ppbv lower than observed. During afternoon hours, the model over-predicts NO by 0.05–0.1 ppbv throughout the canopy. Again, the increase in the soil NO_x flux exerted little influence on the above-canopy morning NO peak formation.

– **O_3**. Regardless of the changes in soil emission rates, the model reasonably predicted absolute O_3 levels, the mixing ratio profiles of O_3, and the timing of the breakup of the nighttime O_3 gradient at sunrise. The SCM underestimated O_3 mixing ratios in the understory layer at sunrise (6:00–9:00 EST hours) and during the late evening and nighttime (18:00–24:00 EST hours). This effect may be related to an overestimation of canopy sinks (e.g. foliage or soil deposition, chemical destruction) or an underestimation of downward turbulent transport inside the canopy (Fig. 7, Sect. 5.1).

5.2.2 Foliage emissions

Hanson and Lindberg (1991) compiled a report showing evidence for deposition of NO_x onto surfaces such as leaves, bark, and soil. It is possible that residual NO_2 could be "trapped" in the canopy via deposition onto leaves. At sunrise, the deposited NO_2, either as NO_2 or in the form of HONO or HNO_3, would undergo photolysis to ultimately create NO above the canopy. The sensitivity of NO_x, NO, and O_3 to a foliage NO_x

ACPD
12, 32515–32564, 2012

emission flux is shown in Fig. 10. The foliage NO_x emission rates are based on leaf nitrate content reported by Zhou et al. (2011) (see Table 1), where we assumed that photolysis of nitrate on the surface of the leaves results in foliage NO_2 and HONO emissions (hence, referred to as foliage NO_x emissions). The simulated cases include a "zero" foliage NO_x emissions flux (0×; Fig. 10b), an assumed foliage NO_x emissions flux based on the reported leaf nitrate value (0.83 nmol cm^{-2}, Table 1) (1×; Fig. 10c), and increased foliage NO_x emission fluxes based on 10 and 25 times increases in the reported leaf nitrate levels (10× and 25×, see Table 1; Fig. 10d, e). In Fig. 10b–e, a positive delta value mean that the model has overestimated the mixing ratio, while a negative delta implies an underestimation in the simulated mixing ratio value.

- **NO_x**. The increase in foliage NO_x emissions causes increasing NO_x levels during the sunlit daytime hours, with most of this NO_x growth seen in the understory layer where NO_x accumulates due to slower removal by transport, chemistry, and deposition. For the 10× and 25× simulation cases, resulting NO_x levels are far above the observed data. These comparisons do not provide evidence that foliage emission have a determining influence on the above-canopy morning NO_x peak.

- **NO**. NO results are similar to NO_x, except that the effect on NO is not constrained to the understory layer but is notable throughout the canopy and above-canopy layer. Yet again, increasing the foliage NO_x emissions rate above the default value yields atmospheric NO levels that exceed the observations.

- **O_3**. Increasing the foliage NO_x flux had little influence on the O_3 mixing ratios. Likewise to the sensitivity of soil NO emissions (Sect. 5.2.1), the underestimation of O_3 in the understory layer during sunrise and late evening hours seen in the comparison between the observed and the simulated values is insensitive to changes in foliage NO_x flux.

ACPD
12, 32515–32564, 2012

5.2.3 Leaf-scale bidirectional exchanges of NO_2

To further diagnose the contribution of the different processes that influence the diurnal variability in NO_x, the simulated process tendencies for the default conditions (expressed in ppbv hr^{-1}) are shown for the crown layer in Fig. 11a, and for the understory layer in Fig. 11b. From Fig. 11a it can be inferred that changes in the crown layer NO_x mixing ratio are dominated by daytime downward turbulent transport into the canopy (shown as positive turbulence tendency). This downward transport compensates for chemical destruction and dry deposition. Figure 11b also shows the contribution from soil emission, which provides a constant but relatively minor contribution in the overall net tendency. This confirms the low sensitivity of NO_x at UMBS to the soil emission source. It is interesting to see that the net tendency after sunrise appears to be controlled primarily by turbulent transport and dry deposition (Fig. 11). Meanwhile, the chemistry becomes a relevant sink ~ 1.5 h after sunrise. The SCM calculates NO_x dry deposition in the multi-layer canopy model from the leaf uptake resistance. This leaf uptake resistance includes non-stomatal and stomatal resistances, and it is calculated from radiation and moisture status in series with an assumed mesophyll resistance. In the default setup of the SCM, the NO_2 mesophyll resistance has a value such that the NO_2 dry deposition to vegetation is $\sim 2/3$ the O_3 dry deposition velocity, while NO leaf uptake is negligible (Ganzeveld and Lelieveld, 1995).

However, studies have shown that there exists a NO_2 compensation point defined as the ambient NO_2 mixing ratio at which the net exchange between a plant and the atmosphere is zero (e.g. Rondon et al., 1993; Rondon and Granat, 1994; Lerdau et al., 2000; Ganzeveld et al., 2002b; Chaparro-Suarez et al., 2011). The NO_2 compensation point can be viewed as a dynamic process. The canopy foliage can become a source or a sink depending on the ambient NO_2 mixing ratio. This contrasts the foliage emissions via nitrate photolysis, described in Sect. 5.2.2, which always function as a source term (i.e. always resulting in a positive NO_x flux). The NO_2 gas exchange is a pure

ACPD
12, 32515–32564, 2012

physical process, solely driven by ambient air mixing ratio levels. The compensation point mechanism was added on top of the foliage emission flux in these simulations.

Recognizing the potential importance of a NO_2 compensation point an additional simulation taking this NO_2 compensation point into account was conducted. A leaf-scale NO_2 compensation point of 1 ppbv was used in the simulation. This compensation point value was selected after conducting sensitivity analysis (not shown) aiming to reproduce the observed trace gas levels throughout the day. With inclusion of this NO_2 compensation point in the SCM, a relatively large NO_x foliage emissions flux, exceeding the dry deposition term, was simulated (Fig. 12). Having this compensation point reverses the net tendency at ~ 06:00 EST from a negative (see Fig. 11a) to a positive tendency (Fig. 12). Comparing Fig. 11a and Fig. 12, one would expect the turbulence tendency to be the same for both simulations. However, inclusion of a NO_2 compensation point changes the sources and sinks; consequently, this changes the mixing ratios in the simulation. Therefore, the turbulent transport tendency (along with the concentration gradients and fluxes) will change accordingly, but the turbulent transport term, derived from the eddy diffusivity, in the SCM remained the same for the two cases. The simulated increases in atmospheric NO_x and NO mixing ratios associated with this 1 ppbv NO_2 compensation point is illustrated in Fig. 13. First of all, there is an improved simulation of absolute mixing ratios with maximum increases in NO_x of ~ 0.3 ppbv and in NO ~ 0.05 ppbv in the crown layer (Fig. 13c). Moreover, the better match in the timing of the NO_x and NO maxima associated with these changes in leaf-level NO_2 exchange (i.e. the NO_2 compensation point) points towards this effect having a possible important contribution to the above canopy morning NO maximum.

At this time, there are no leaf-level experimental data available from this site to further substantiate the assumption that NO_2 compensation point might play an important role in the dynamics of NO_x at UMBS. However, after demonstrating the significant changes in absolute mixing ratios as well as temporal variability in NO_x, studies of the role of this foliage source of NO_x, warrant further investigation.

ACPD
12, 32515–32564, 2012

5.3 Synthesis

Based on our air mass transport analysis, we conclude that advection and entrainment of polluted air masses play an integral role in the observed NO_x dynamics at UMBS in addition to local scale atmosphere-biosphere exchanges. Advection of NO_x and O_3 in the model was achieved by nudging the model layer above the canopy towards observation. Nudging the model allows us to assess the effects that local processes and non-local sources of pollution have on the temporal variability in NO_x and O_3 within and below the canopy under observed conditions. As such, our study – including the presented model analysis – adds to that by Alaghmand et al. (2011), who analyzed the relative contributions of in-canopy air versus the supply of NO_x and other pollutants through advection and entrainment of residual layer air masses at UMBS solely based on observations.

The 3-h lag in the NO maximum after sunrise suggests that this maximum could be associated (1) with entrainment of polluted air masses higher up in the residual layer or (2) with advection of pollution from an anthropogenic source area at an upwind distance resembling a 3-h transport time. Observed vertical gradients and meteorological data imply mixing ratios in the understory layer are depleted by chemical reaction and deposition and replenished by downward mixing of elevated mixing ratios from above the canopy. Alaghmand et al. (2011) suggested that downward mixing of localized polluted air masses did not contribute to the morning NO_x maximum. Rather, they proposed that long-range transport of aged polluted air masses do explain the observed NO_x peak. In cases where the air mass did not flow through major sources of NO_x, they attributed the morning NO_x maximum to local soil NO_x emissions. Alaghmand et al. (2011) found that in the early morning hours (hours prior to 06:00 EST) ~ 57 % of the time, NO_x mixing ratios were greater below than above canopy. Thus, they postulated that there is sufficient accumulation of NO_x below canopy and if this NO_x was to mix upward with the breakdown of the nocturnal boundary layer, it would contribute to the observed NO_x maximum at sunrise. However, our observations and simulations showed little or

ACPD
12, 32515–32564, 2012

no accumulation of NO in the understory layer under UMBS conditions, thus providing no evidence that soil NO emissions could influence the morning NO_x maximum.

Munger et al. (1996) showed that HNO_3 could mix into the canopy layer at sunrise with the breakdown of the nocturnal boundary layer, but efficient deposition of total oxidized nitrogen (NO_y) would prevent HNO_3 to accumulate in the understory layer. If there was a sufficient amount of HNO_3 (or HONO) present on the surface of the canopy leaves, then photolysis upon sunrise could account for some of the increase in NO_x mixing ratios during that time. Our simulations showed that foliage emissions of NO_x via nitrate photolysis alone could not explain the observed NO_x maximum in the morning. In fact, it appears that the diurnal behavior is not properly represented including this foliage NO_x source from nitrate photolysis. However, when considering the NO_2 compensation point at the leaf-scale of the canopy, our simulated results were closer to the observed, suggesting that the NO_2 compensation point mechanism may be important in explaining the dynamics of NO_x at UMBS.

The below-to-above canopy O_3 dynamics in August reflects the combined role of in-canopy and boundary layer photochemistry and turbulent transport resulting in entrainment of free tropospheric air masses enhanced in O_3 compensating for canopy deposition. During the night, O_3 titration through its reaction with NO reduces below canopy O_3 levels. However, the observed NO levels below canopy were generally about two orders of magnitude smaller compared to O_3 implying that other sinks, e.g. ozonolysis of very reactive BVOCs (Kurpius and Goldstein, 2003), and dry deposition explain the apparent significant ozone sink in the understory. Bryan et al. (2012) also conducted a model study for this site and concluded that deposition was the primary sink for ozone in the canopy layer.

The simulation of dry deposition in our model is based on the selected fixed cuticular, soil and other substrate resistances according to Ganzeveld and Lelieveld (1995). Recent studies (e.g. Zhang et al., 2002; Altimir et al., 2004, 2006) have shown a potentially important role of non-stomatal uptake of O_3 as a function of moisture conditions. To investigate the potential impact of such an enhanced removal by wet surfaces, we

ACPD
12, 32515–32564, 2012

conducted an additional simulation in which we used the relative humidity (RH) of the simulated surface layer as a proxy for canopy wetness (Altimir et al., 2006) (note that the model actually calculates the wet skin fraction, i.e. the fraction of vegetation that is wetted by dewfall and rain interception). We introduced a reduced cuticular resistance scaled between the default maximum resistance of $10^5\,s\,m^{-1}$ for a RH < 70 % and an assumed leaf-scale minimum cuticular resistance of $1500\,s\,m^{-1}$ for a RH > 95 %; in between a RH of 70–95 %, a linear scaling between the minimum and maximum resistance was applied. Selection of the minimum cuticular resistance is based on the reported canopy-scale $V_{d_{O_3}}$ between 0.1 and $0.3\,cm\,s^{-1}$ (Altimir et al., 2006, and references therein), resembling a canopy uptake resistance on the order of $500\,s\,m^{-1}$, and an LAI for this site on the order of 3–3.5 $m^2\,m^{-2}$. Applying this substantially smaller non-stomatal uptake resistance as a function of RH resulted in simulated canopy O_3 mixing ratios, which were up to ∼ 13 ppbv, smaller compared to the observed mixing ratios during nocturnal conditions. This indicates that this enhanced O_3 removal mechanism might not apply to this site. However, it is known that non-stomatal ozone conductance represents over half of the total ozone flux at this site (Hogg et al., 2007). It is uncertain what drives the non-stomatal uptake of ozone. Kurpius and Goldstein (2003) suggested that this would be driven by temperature dependence in BVOC emissions in which ozone scavenging BVOCs would remove the ozone. In any case, our measurements do not allow us to partition between stomatal and non-stomatal uptake, and determining the drivers of the non-stomatal uptake is beyond the scope of this study.

Differences between the daytime August and November O_3 mixing ratios could reflect the combined effect of different boundary layer dynamics (see Fig. 3), with a reduced entrainment of free troposphere air masses enriched in O_3 in November compared to August. A reduced photochemistry in November is partly compensated by a reduced November O_3 sink associated with a decrease in dry deposition.

In summary, the observed morning NO_x maximum appears to be caused by (1) the photolysis of NO_2 from anthropogenic origin, which is supplied by advection and downward transport or (2) the foliage NO_x emissions associated with a NO_2 compensation

ACPD
12, 32515–32564, 2012

point. The latter hypothesis should be futher substantiated by studies of NO_2 bidirectional fluxes at the leaf-level for vegetation found at UMBS.

6 Conclusions

We examined the dynamical behavior in NO_x and O_3 at a deciduous forest site at UMBS. We combined concentration gradient and micrometeorological measurements with a canopy-boundary layer exchange model for a detailed analysis on the role of biogenic emissions, dry deposition, chemistry, turbulent transport, and advection in the observed NO_x and O_3 mixing ratio changes. The NO mixing ratio profile data and SCM runs did not support the hypothesis that soil NO emissions were the cause of the morning NO_x maximum. Sensitivity analyses of the SCM also showed that foliage NO_x emissions via nitrate photolysis cannot explain the observed morning NO maximum above the canopy. However, foliage emissions associated with the existence of an NO_2 compensation point resulted in simulation of absolute mixing ratios and peak timing of NO_x closer to observations, which suggests that this could explain the observed morning NO maximum above the canopy. The sensitivity analysis of the SCM and the analysis of air mass advection suggest that despite UMBS being located in a relatively remote area far from major urban sites, most of the NO_x seen at UMBS is of non-local anthropogenic origin and that its impact is significant on the chemistry observed at the site.

To understand the dynamics of NO_x at UMBS, not only should we consider large scale advection, boundary layer dynamics, and entrainment, we should consider leaf-scale processes as biologically mitigated processes seem to contribute to the observed NO_x dynamics at UMBS. Therefore, more studies on leaf-scale processes and their effect on the biosphere-atmosphere exchange are needed at this site.

ACPD
12, 32515–32564, 2012

Supplementary material related to this article is available online at: http://www.atmos-chem-phys-discuss.net/12/32515/2012/acpd-12-32515-2012-supplement.zip.

Acknowledgements. Thanks are due to S. Garrity for assistance with the experimental setup on the AmeriFlux tower and to K. Mauer for providing the AmeriFlux turbulence data. The lead author and this research were sponsored through the NSF-IGERT Biosphere-Atmosphere Research and Training (BART) Fellowship administrated by the University of Michigan (NSF award #0504552). Work on this research was also supported by funding from NSF award AGS #0904139.

References

Alaghmand, M., Shepson, P. B., Starn, T. K., Jobson, B. T., Wallace, H. W., Carroll, M. A., Bertman, S. B., Lamb, B., Edburg, S. L., Zhou, X., Apel, E., Riemer, D., Stevens, P., and Keutsch, F.: The Morning NO_x maximum in the forest atmosphere boundary layer, Atmos. Chem. Phys. Discuss., 11, 29251–29282, doi:10.5194/acpd-11-29251-2011, 2011. 32517, 32530, 32534, 32539

Andreae, M. O., Artaxo, P., Brandao, C., Carswell, F. E., Ciccioli, P., da Costa, A. L., Culf, A. D., Esteves, J. L., Gash, J. H. C., Grace, J., Kabat, P., Lelieveld, J., Malhi, Y., Manzi, A. O., Meixner, F. X., Nobre, A. D., Nobre, C., Ruivo, M. d. L. P., Silva-Dias, M. A., Stefani, P., Valentini, R., von Jouanne, J., and Waterloo, M. J.: Biogeochemical cycling of carbon, water, energy, trace gases, and aerosols in Amazonia: the LBA-EUSTACH experiments, J. Geophys. Res.-Atmos., 107, 8066, doi:10.1029/2001JD000524, 2002. 32517

Atkinson, R., Baulch, D. L., Cox, R. A., Crowley, J. N., Hampson, R. F., Hynes, R. G., Jenkin, M. E., Rossi, M. J., and Troe, J.: Evaluated kinetic and photochemical data for atmospheric chemistry: Volume I – gas phase reactions of O_x, HO_x, NO_x and SO_x species, Atmos. Chem. Phys., 4, 1461–1738, doi:10.5194/acp-4-1461-2004, 2004. 32521

Altimir, N., Tuovinen, J.-P., Vesala, T., Kulmala, M., and Hari, P.: Measurements of ozone removal by Scots pine shoots: calibration of a stomatal uptake model including the non-

ACPD

12, 32515–32564, 2012

stomatal component, Atmos. Environ., 38, 2387–2398, doi:10.1016/j.atmosenv.2003.09.077, 2004. 32540

Altimir, N., Kolari, P., Tuovinen, J.-P., Vesala, T., Bäck, J., Suni, T., Kulmala, M., and Hari, P.: Foliage surface ozone deposition: a role for surface moisture?, Biogeosciences, 3, 209–228, doi:10.5194/bg-3-209-2006, 2006. 32540, 32541

Bakwin, P. S., Wofsy, S. C., Fan, S. M., Keller, M., Trumbore, S. E., and Dacosta, J. M.: Emission of nitric-oxide (NO) from tropical forest soils and exchange of NO between the forest canopy and atmospheric boundary-layers, J. Geophys. Res.-Atmos., 95, 16755–16764, 1990. 32517

Bakwin, P. S., Jacob, D. J., Wofsy, S. C., Munger, J. W., Daube, B. C., Bradshaw, J. D., Sandholm, S. T., Talbot, R. W., Singh, H. B., Gregory, G. L., and Blake, D. R.: Reactive nitrogen-oxides and ozone above a taiga, J. Geophys. Res.-Atmos., 99, 1927–1936, 1994. 32517

Brodin, M., Helmig, D., and Oltmans, S.: Seasonal ozone behavior along an elevation gradient in the Colorado Front Range Mountains, Atmos. Environ., 44, 5305–5315, doi:10.1016/j.atmosenv.2010.06.033, 2010. 32519

Bryan, A. M., Bertman, S. B., Carroll, M. A., Dusanter, S., Edwards, G. D., Forkel, R., Griffith, S., Guenther, A. B., Hansen, R. F., Helmig, D., Jobson, B. T., Keutsch, F. N., Lefer, B. L., Pressley, S. N., Shepson, P. B., Stevens, P. S., and Steiner, A. L.: In-canopy gas-phase chemistry during CABINEX 2009: sensitivity of a 1-D canopy model to vertical mixing and isoprene chemistry, Atmos. Chem. Phys., 12, 8829–8849, doi:10.5194/acp-12-8829-2012, 2012. 32540

Carleton, L., Carrol, M. A., and Hogg, A.: NO flux from soils surrounding PROPHET tower at UMB S.: Deep Blue at the University of Michigan, available at: http://hdl.handle.net/2027.42/54978 (last accessed 29 April 2011), 2003. 32533, 32534

Carroll, M. A. and Thompson, A. M.: NO_x in the non-urban troposphere, in: Progress and Problems in Atmospheric Chemistry, vol. 3, edited by: Barker, J. R., World Scientific, River Edge, NJ, 198–226, 1995. 32517

Carroll, M. A., Bertman, S. B., and Shepson, P. B.: Overview of the program for research on oxidants: photochemistry, emissions, and transport (PROPHET) summer 1998 measurements intensive, J. Geophys. Res.-Atmos., 106, 24275–24288, 2001. 32517

Chaparro-Suarez, I. G., Meixner, F. X., and Kesselmeier, J.: Nitrogen dioxide (NO_2) uptake by vegetation controlled by atmospheric concentrations and plant stomatal aperture, Atmos. Environ., 45, 5742–5750, doi:10.1016/j.atmosenv.2011.07.021, 2011. 32537

ACPD
12, 32515–32564, 2012

Cooper, O. R., Moody, J. L., Thornberry, T. D., Town, M. S., and Carroll, M. A.: PROPHET 1998 meteorological overview and air-mass classification, J. Geophys. Res.-Atmos., 106, 24289–24299, 2001. 32527, 32530

Crutzen, P. J.: Influence of nitrogen oxides on atmospheric ozone content, Q. J. Roy. Meteor. Soc., 96, 320–325, 1970. 32517

Crutzen, P. J. and Lelieveld, J.: Human impacts on atmospheric chemisty, Annu. Rev. Earth Pl. Sc., 29, 17–45, 2001. 32517

Demerjian, K. L.: A review of national monitoring networks in North America, Atmos. Environ., 34, 1861–1884, 2000. 32519

Farmer, D. K. and Cohen, R. C.: Observations of HNO_3, ΣAN, ΣPN and NO_2 fluxes: evidence for rapid HO_x chemistry within a pine forest canopy, Atmos. Chem. Phys., 8, 3899–3917, doi:10.5194/acp-8-3899-2008, 2008. 32517

Fuchs, H., Holland, F., and Hofzumahaus, A.: Measurement of tropospheric RO_2 and HO_2 radicals by a laser-induced fluorescence instrument, Rev. Sci. Instrum., 79, 084104, doi:10.1063/1.2968712, 2008. 32521

Ganzeveld, L. and Lelieveld, J.: Dry deposition parameterization in a chemistry general-circulation model and its influence on the distribution of reactive trace gases, J. Geophys. Res.-Atmos., 100, 20999–21012, 1995. 32523, 32537, 32540, 32550

Ganzeveld, L. N., Lelieveld, J., Dentener, F. J., Krol, M. C., and Roelofts, G. J.: Atmosphere-biosphere trace gas exchanges simulated with a single-column model, J. Geophys. Res.-Atmos., 107, 4297, doi:10.1029/2001JD000684, 2002a. 32522

Ganzeveld, L. N., Lelieveld, J., Dentener, F. J., Krol, M. C., Bouwman, A. F., and Roelofs, G. J.: Global soil-biogenic NO_x emissions and the role of canopy processes, J. Geophys. Res.-Atmos., 107, 4298, doi:10.1029/2001JD001289, 2002b. 32537

Ganzeveld, L., Klemm, O., Rappenglueck, B., and Valverde-Canossa, J.: Evaluation of meteorological parameters over a coniferous forest in a single-column chemistry-climate model, Atmos. Environ., 40, 21–27, doi:10.1016/j.atmosenv.2006.01.061, 2006. 32522, 32524, 32550

Ganzeveld, L., Eerdekens, G., Feig, G., Fischer, H., Harder, H., Königstedt, R., Kubistin, D., Martinez, M., Meixner, F. X., Scheeren, H. A., Sinha, V., Taraborrelli, D., Williams, J., Vilà-Guerau de Arellano, J., and Lelieveld, J.: Surface and boundary layer exchanges of volatile organic compounds, nitrogen oxides and ozone during the GABRIEL campaign, Atmos. Chem. Phys., 8, 6223–6243, doi:10.5194/acp-8-6223-2008, 2008. 32522

ACPD
12, 32515–32564, 2012

Gough, C. M., Vogel, C. S., Harrold, K. H., George, K., and Curtis, P. S.: The legacy of harvest and fire on ecosystem carbon storage in a north temperate forest, Glob. Change Biol., 13, 1935–1949, doi:10.1111/j.1365-2486.2007.01406.x, 2007. 32518

Grunhage, L., Dammgen, U., Erisman, J. W., Luttich, M., Hanewald, K., Jager, H. J., Freitag, K., Baltrusch, M., and Liebl, K.: Atmospheric nitrogen dynamics in Hesse, Germany: the challenge and its potential solution, Landbauforsch. Volk., 52, 219–228, 2002. 32517

Guenther, A., Hewitt, C. N., Erickson, D., Fall, R., Geron, C., Graedel, T., Harley, P., Klinger, L., Lerdau, M., McKay, W. A., Pierce, T., Scholes, B., Steinbrecher, R., Tallamraju, R., Taylor, J., and Zimmerman P.: A global-model of natural volatile organic-compound emissions, J. Geophys. Res.-Atmos., 100, 8873–8892, doi:10.1029/94JD02950, 1995. 32523

Guenther, A., Karl, T., Harley, P., Wiedinmyer, C., Palmer, P. I., and Geron, C.: Estimates of global terrestrial isoprene emissions using MEGAN (Model of Emissions of Gases and Aerosols from Nature), Atmos. Chem. Phys., 6, 3181–3210, doi:10.5194/acp-6-3181-2006, 2006. 32523

Hanson, P. J. and Lindberg, S. E.: Dry deposition of reactive nitrogen-compounds – a review of leaf, canopy and non-foliar measurements, Atmos. Environ., 25, 1615–1634, 1991. 32535

Hauglustaine, D., Emmons, L., Newchurch, M., Brasseur, G., Takao, T., Matsubara, K., Johnson, J., Ridley, B., Stith, J., and Dye, J.: On the role of lightning NO_x in the formation of tropospheric ozone plumes: a global model perspective, J. Atmos. Chem., 38, 277–294, 2001. 32517

Hogg, A., Uddling, J., Ellsworth, D., Carroll, M. A., Pressley, S., Lamb, B., and Vogel, C.: Stomatal and non-stomatal fluxes of ozone to a northern mixed hardwood forest, Tellus B, 59, 514–525, doi:10.1111/j.1600-0889.2007.00269.x, 2007. 32541

Hollinger, D. Y., Ollinger, S. V., Richardson, A. D., Meyers, T. P., Dail, D. B., Martin, M. E., Scott, N. A., Arkebauer, T. J., Baldocchi, D. D., Clark, K. L., Curtis, P. S., Davis, K. J., Desai, A. R., Dragoni, D., Goulden, M. L., Gu, L., Katul, G. G., Pallardy, S. G., Paw U, K. T., Schmid, H. P., Stoy, P. C., Suyker, A. E., and Verma, S. B.: Albedo estimates for land surface models and support for a new paradigm based on foliage nitrogen concentration, Glob. Change Biol., 16, 696–710, doi:10.1111/j.1365-2486.2009.02028.x, 2010. 32550

Jacob, D. J.: Heterogeneous chemistry and tropospheric ozone, Atmos. Environ., 34, 2131–2159, 2000. 32517

ACPD
12, 32515–32564, 2012

Kurpius, M. R. and Goldstein, A. H.: Gas-phase chemistry dominates O_3 loss to a forest, implying a source of aerosols and hydroxyl radicals to the atmosphere, Geophys. Res. Lett., 30, 1371, doi:10.1029/2002GL016785, 2003. 32540, 32541

Lerdau, M. T., Munger, L. J., and Jacob, D. J.: The NO_2 flux conundrum, Science, 289, 2291–2293, doi:10.1126/science.289.5488.2291, 2000. 32537

Mosier, A. R., Bleken, M. A., Chaiwanakupt, P., Ellis, E. C., Freney, J. R., Howarth, R. B., Matson, P. A., Minami, K., Naylor, R., Weeks, K. N., and Zhu, Z. L.: Policy implications of human-accelerated nitrogen cycling, Biogeochemistry, 52, 281–320, 2001. 32517

Munger, J. W., Wofsy, S. C., Bakwin, P. S., Fan, S. M., Goulden, M. L., Daube, B. C., Goldstein, A. H., Moore, K. E., and Fitzjarrald, D. R.: Atmospheric deposition of reactive nitrogen oxides and ozone in a temperate deciduous forest and a subarctic woodland, 1: measurements and mechanisms, J. Geophys. Res.-Atmos., 101, 12639–12657, 1996. 32517, 32540

Nave, L. E., Gough, C. M., Maurer, K. D., Bohrer, G., Hardiman, B. S., Le Moine, J., Munoz, A. B., Nadelhoffer, K. J., Sparks, J. P., Strahm, B. D., Vogel, C. S., and Curtis, P. S.: Disturbance and the resilience of coupled carbon and nitrogen cycling in a north temperate forest, J. Geophys. Res., 116, G04016, doi:10.1029/2011JG001758, 2011. 32534

Ortega, J., Helmig, D., Guenther, A., Harley, P., Pressley, S., and Vogel, C.: Flux estimates and OH reaction potential of reactive biogenic volatile organic compounds (BVOCs) from a mixed northern hardwood forest, Atmos. Environ., 41, 5479–5495, doi:10.1016/j.atmosenv.2006.12.033, 2007. 32523, 32550

Parrish, D. D., Buhr, M. P., Trainer, M., Norton, R. B., Shimshock, J. P., Fehsenfeld, F. C., Anlauf, K. G., Bottenheim, J. W., Tang, Y. Z., Wiebe, H. A., Roberts, J. M., Tanner, R. L., Newman, L., Bowersox, V. C., Olszyna, K. J., Bailey, E. M., Rodgers, M. O., Wang, T., Berresheim, H., Roychowdhury, U. K., and Demerjiani, K. L.: The total reactive oxidized nitrogen levels and the partitioning between the individual-species at 6 rural sites in Eastern North-America, J. Geophys. Res.-Atmos., 98, 2927–2939, doi:10.1029/92JD02384, 1993. 32517

Pressley, S., Lamb, B., Westberg, H., Flaherty, J., Chen, J., and Vogel, C.: Long-term isoprene flux measurements above a northern hardwood forest, J. Geophys. Res.-Atmos., 110, D07301, doi:10.1029/2004JD005523, 2005. 32523

Rondon, A. and Granat, L.: Studies on the dry deposition of NO_2 to coniferous tree species at low NO_2 concentrations, Tellus, 46, 339–352, 1994. 32537

Rondon, A., Johansson, C., and Granat, L.: Dry deposition of nitrogen dioxide and ozone to coniferous forests, J. Geophys. Res., 98, 5159–5172, 1993. 32537

ACPD
12, 32515–32564, 2012

Rummel, U., Ammann, C., Gut, A., Meixner, F. X., and Andreae, M. O.: Eddy covariance measurements of nitric oxide flux within an Amazonian rain forest, J. Geophys. Res.-Atmos., 107, 8050, doi:10.1029/2001JD000520, 2002. 32517

Schmid, H. P., Su, H. B., Vogel, C. S., and Curtis, P. S.: Ecosystem-atmosphere exchange of carbon dioxide over a mixed hardwood forest in northern lower Michigan, J. Geophys. Res.-Atmos., 108, 4417, doi:10.1029/2002JD003011, 2003. 32518, 32519, 32522, 32550, 32552

Spicer, C. W.: The distribution of oxidized nitrogen in urban air, Sci. Total Environ., 24, 183–192, 1982. 32519

Steinbacher, M., Zellweger, C., Schwarzenbach, B., Bugmann, S., Buchmann, B., Ordonez, C., Prevot, A. S. H., and Hueglin, C.: Nitrogen oxide measurements at rural sites in Switzerland: bias of conventional measurement techniques, J. Geophys. Res.-Atmos., 112, D11307, doi:10.1029/2006JD007971, 2007. 32519

Thornberry, T., Carroll, M. A., Keeler, G. J., Sillman, S., Bertman, S. B., Pippin, M. R., Ostling, K., Grossenbacher, J. W., Shepson, P. B., Cooper, O. R., Moody, J. L., and Stockwell, W. R.: Observations of reactive oxidized nitrogen and speciation of NO_y during the PROPHET summer 1998 intensive, J. Geophys. Res.-Atmos., 106, 24359–24386, doi:10.1029/2000JD900760, 2001. 32517, 32530

United States Department of Agriculture Forest Service: Strategy for the 90's for USDA Forest Service Research, Technical Report, United States Department of Agriculture, Washington, D.C., 1990.

United States Environmental Protection Agency: Clean Air Status and Trends Network (CASTNET) 2009 Annual Report, Annual Report, US Environmental Protection Agency, Washington, D.C., available at: http://epa.gov/castnet/javaweb/docs/annual_report_2009.pdf (last accessed 1 February 2011), 2009. 32517

Vande Kopple, B.: UM Biological Station – Research Resources: Climatology, available at: http://sitemaker.umich.edu/umbs/climatology (last accessed 29 April 2011), 2011. 32518

Villani, M. G., Schmid, H. P., Su, H. B., Hutton, J. L., and Vogel, C. S.: Turbulence statistics measurements in a northern hardwood forest, Bound.-Lay. Meteorol., 108, 343–364, doi:10.1023/A:1024118808670, 2003.

Yienger, J. J. and Levy, H.: Empirical-model of global soil-biogenic NO_x emissions, J. Geophys. Res.-Atmos., 100, 11447–11464, 1995. 32523

Zhang, L. M., Brook, J. R., and Vet, R.: On ozone dry deposition with emphasis on non-stomatal uptake and wet canopies, Atmos. Environ., 36, 4787–4799, 2002. 32540

ACPD
12, 32515–32564, 2012

Zhou, X., Gao, H., He, Y., Huang, G., Bertman, S. B., Civerolo, K., and Schwab, J.: Nitric acid photolysis on surfaces in low-NO_x environments: significant atmospheric implications, Geophys. Res. Lett., 30, 2217, doi:10.1029/2003GL018620, 2003. 32523

Zhou, X. L., Zhang, N., TerAvest, M., Tang, D., Hou, J., Bertman, S., Alaghmand, M., Shepson, P. B., Carroll, M. A., Griffith, S., Dusanter, S., and Stevens, P. S.: Nitric acid photolysis on forest canopy surface as a source for tropospheric nitrous acid, Nat. Geosci., 4, 440–443, doi:10.1038/NGEO1164, 2011. 32536, 32550

ACPD

12, 32515–32564, 2012

Table 1. Model input parameters for the UMBS Ameriflux site.

Parameter	Unit	Value	Reference
Canopy height	m	22	Schmid et al. (2003)
Surface roughness	m	2.2	Schmid et al. (2003)
LAI	$m^2\,m^{-2}$	3.5	Vogel (personal communication, 2010)
Albedo	–	0.15	Hollinger et al. (2010)
Isoprene emis. factor	$\mu g\,C\,g^{-1}\,h^{-1}$	50	Ortega et al. (2007)
Monoterpene emis. factor	$\mu g\,C\,g^{-1}\,h^{-1}$	0.7	Ortega et al. (2007)
Soil NO emis. rate	$ng\,C\,m^{-2}\,s^{-1}$	0.07	Carleton et al. (2003)*
Leaf nitrate conc.	$nmol\,cm^{-2}$	0.83	Zhou et al. (2011)
O_3 soil uptake rate	$cm\,s^{-1}$	0.25	Ganzeveld and Lelieveld (1995)
Synoptic meteorology	–	ECMWF	Ganzeveld et al. (2006)
Chem. initialization	–	NO_x and O_3 mixing ratios	This study

* Unpublished study; Rain event values were excluded from the average because the rainfall for 2008 during the study period was below the normal.

ACPD
12, 32515–32564, 2012

Table 2. UMBS 1979–2010 climatological data for months when measurements were taken.

Month	Temperature (°C)				Precipitation (mm)	
	1979–2010		2008		1979–2010	2008
	Avg. Min	Avg. Max	Min	Max	Avg. Total (±1 std. dev.)	Total
Jul	15.1	25.7	15	25.6	700 (±150)	600
Aug	14.6	24.4	14.4	25.6	850 (±154)	500
Sep	10.3	19.8	10.6	20	880 (±166)	630
Oct	4.3	12.2	4.4	12.2	920 (±178)	310
Dec	−0.71	5.3	0.0	5.0	730 (±123)	680

ACPD
12, 32515–32564, 2012

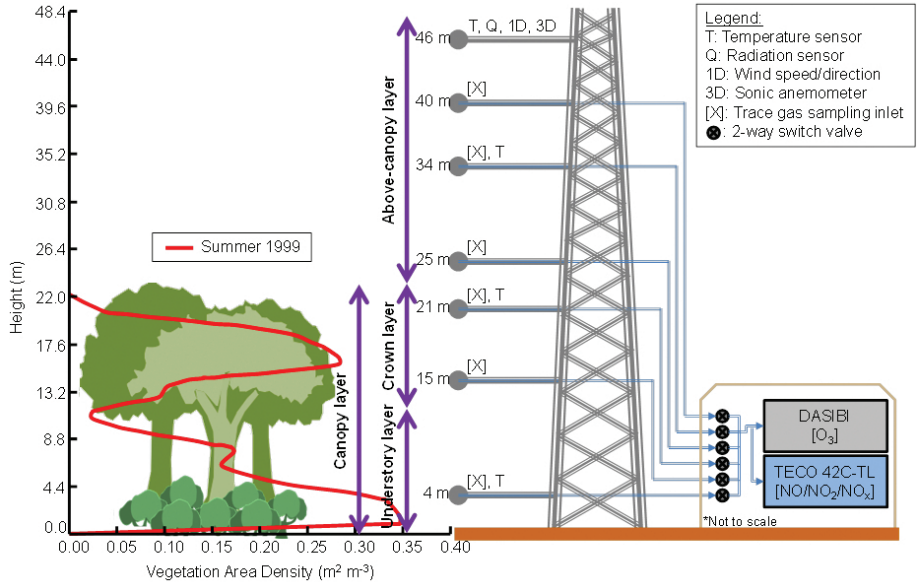

Fig. 1. The forest architecture as vegetation area density profile at UMBS in the summer of 1999, modified from Fig. 2a of Schmid et al. (2003), and a cartoon depiction of the AmeriFlux tower with sensor locations drawn to scale but gas analyzers and housing unit not drawn to scale.

ACPD
12, 32515–32564, 2012

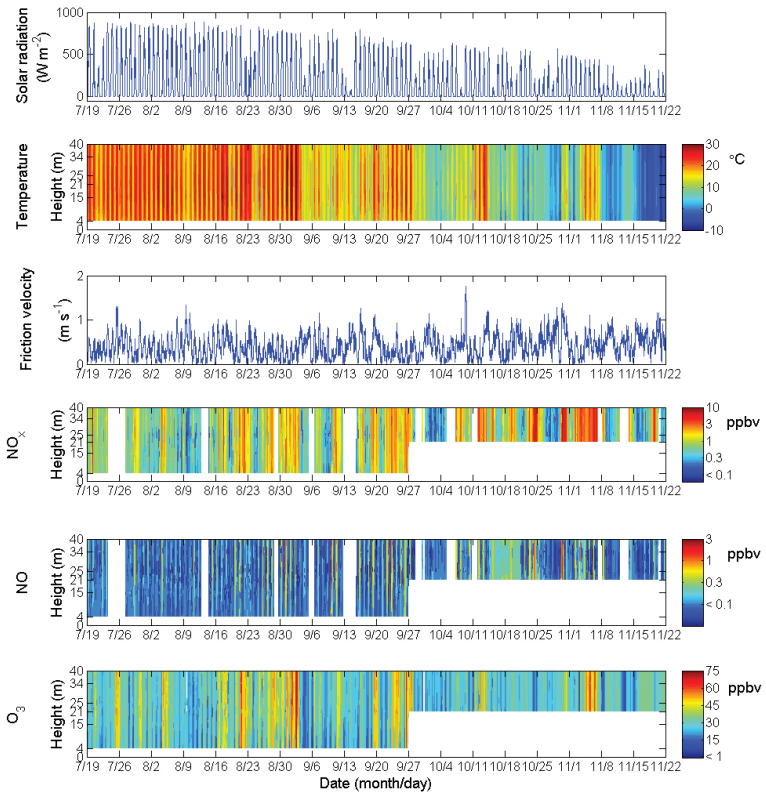

Fig. 2. The evolution of solar radiation, temperature profile, friction velocity, and the mixing ratio profiles of NO_x, NO, and O_3 at the UMBS AmeriFlux site from 19 July to 21 November 2008. Missing data were due to taking the instruments offline for calibrations and repairs and due to running intercomparison tests of the sampling inlets. Gaps in the chemical data below the canopy from 27 September onward were due to failures in the 4 and 15 m switching valves.

ACPD
12, 32515–32564, 2012

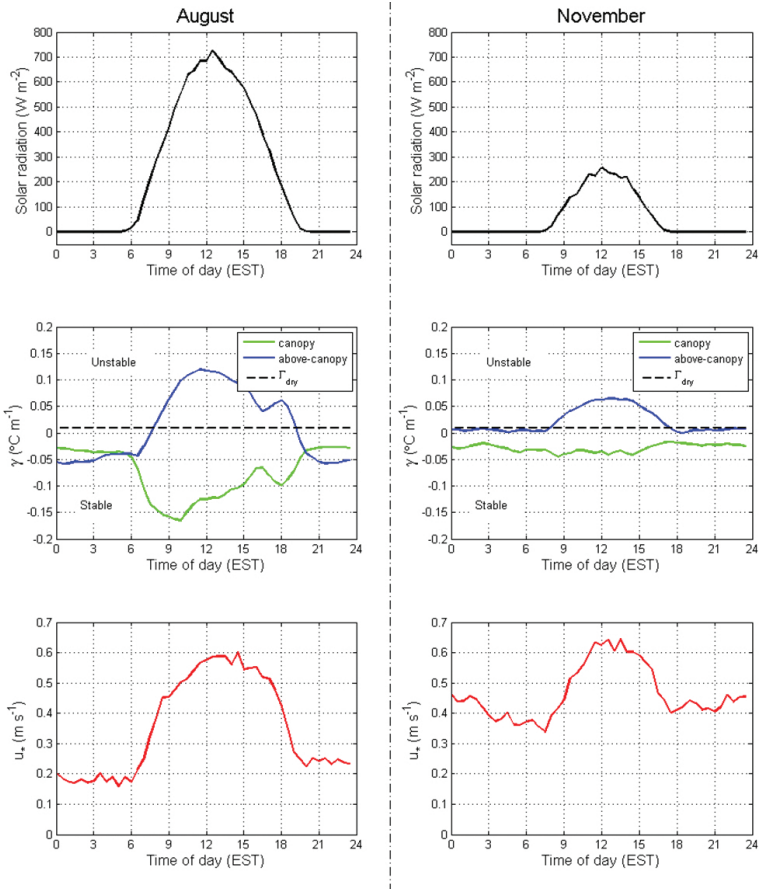

Fig. 3. Mean diurnal cycles of solar radiation, temperature lapse rates (γ), and friction velocity (u_*) in the above-canopy layer at UMBS for August and November 2008. The dotted line in the γ plots denotes the dry adiabatic lapse rate (Γ_{dry}) of 0.0098 °C m^{-1}. $\gamma < \Gamma_{dry}$ is stable, $\gamma = \Gamma_{dry}$ is neutral, and $\gamma > \Gamma_{dry}$ is unstable.

ACPD
12, 32515–32564, 2012

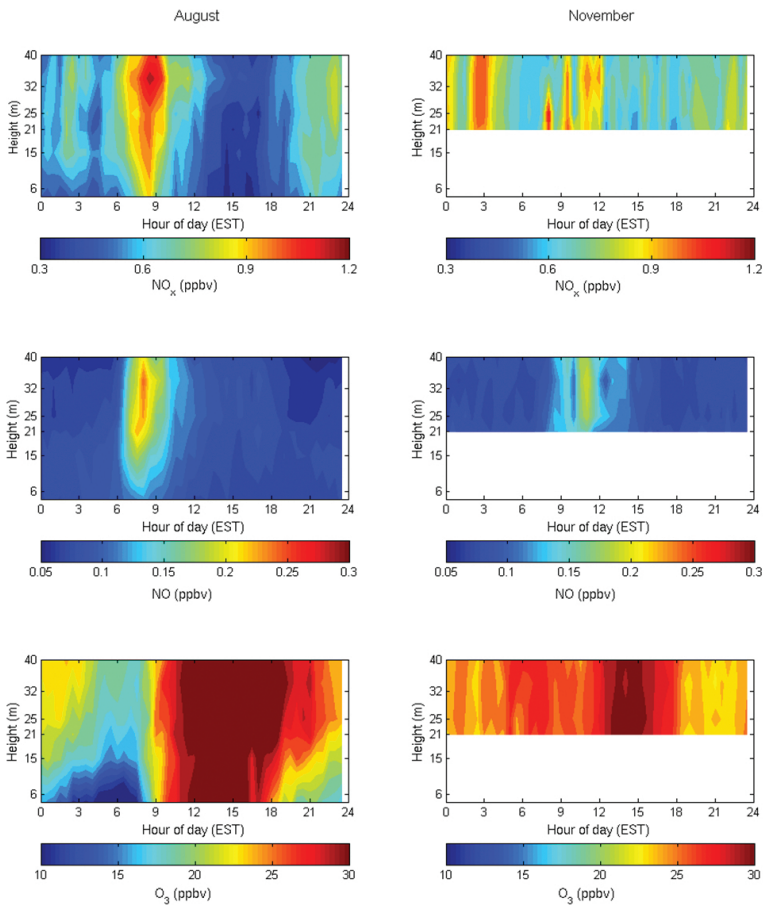

Fig. 4. Mean diurnal cycles of NO_x, NO, and O_3 mixing ratio profiles from the UMBS AmeriFlux site for August and November 2008. The area between the dashed lines in the plots denotes the crown layer. Gaps in the data below the crown layer in November are due to failures in the 4 and 15 m switching valves.

ACPD
12, 32515–32564, 2012

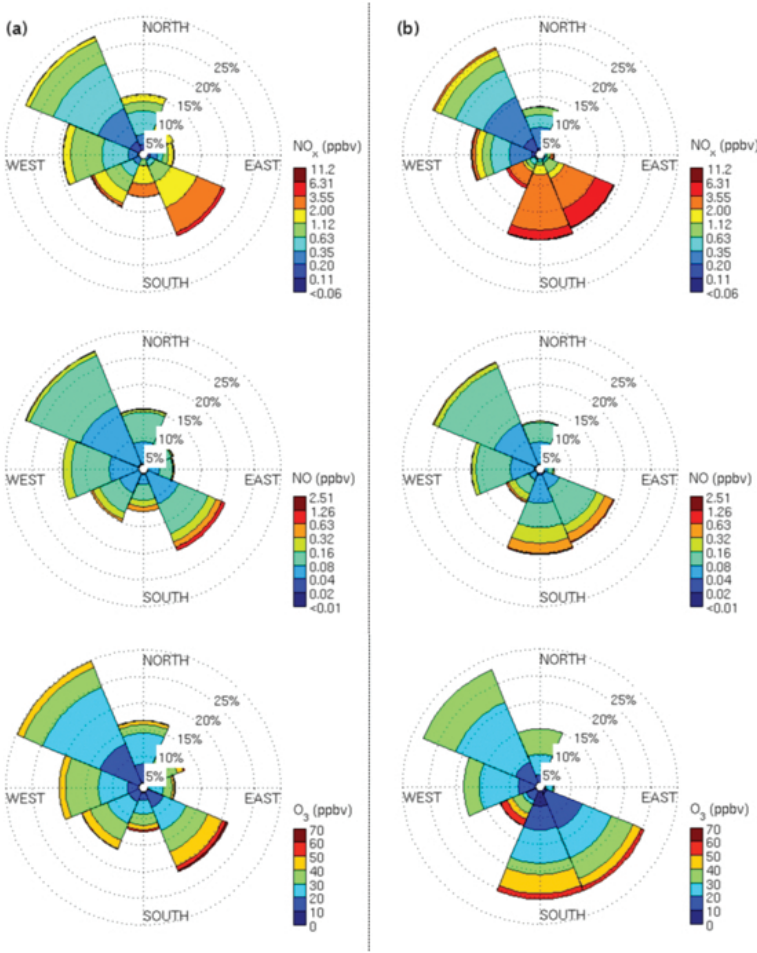

Fig. 5. Wind-pollution rose for NO_x, NO, and O_3 determined for **(a)** August and for **(b)** November using data from the 46 m level wind sensor and 34 m level gas inlet (see Fig. 1).

ACPD
12, 32515–32564, 2012

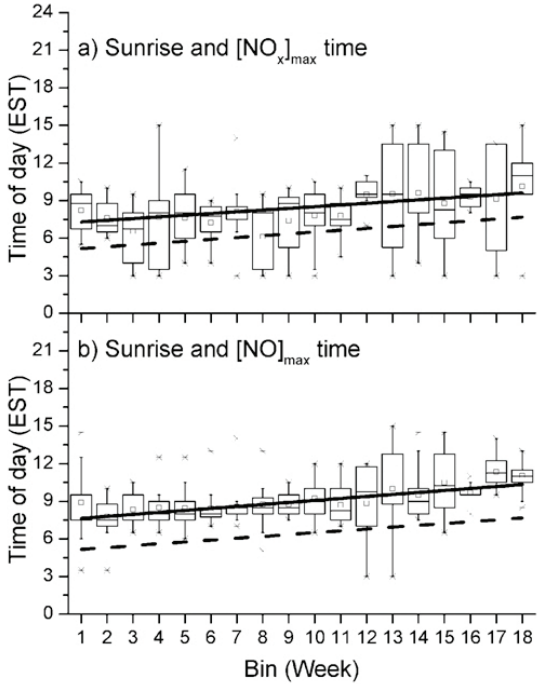

Fig. 6. The relationship between sunrise and time of observed **(a)** NO_x and **(b)** NO maxima from 03:00 to 15:00 EST from each sampling inlets. The dashed lines denote the change in sunrise over 18 weeks (five months) in 2008 at UMBS (regression: $y = 0.147x + 5.01$, $r^2 = 0.999$). Data for 7 days, staring on 19 July were binned together and are displayed as box-and-whisker plots that depict the mean, median, 25 and 75 percentile, and 5 and 95 percentile values. The solid regression lines were fit to the weekly median data. They denote the average change in when the NO_x and the NO maxima were observed [regression: **(a)** $y = 0.135(\mathrm{SE} \pm 0.0355)x + 7.14(\mathrm{SE} \pm 0.384)$, $r^2 = 0.478$ and **(b)** $y = 0.159(\mathrm{SE} \pm 0.0321)x + 7.46(\mathrm{SE} \pm 0.348)$, $r^2 = 0.605$].

ACPD
12, 32515–32564, 2012

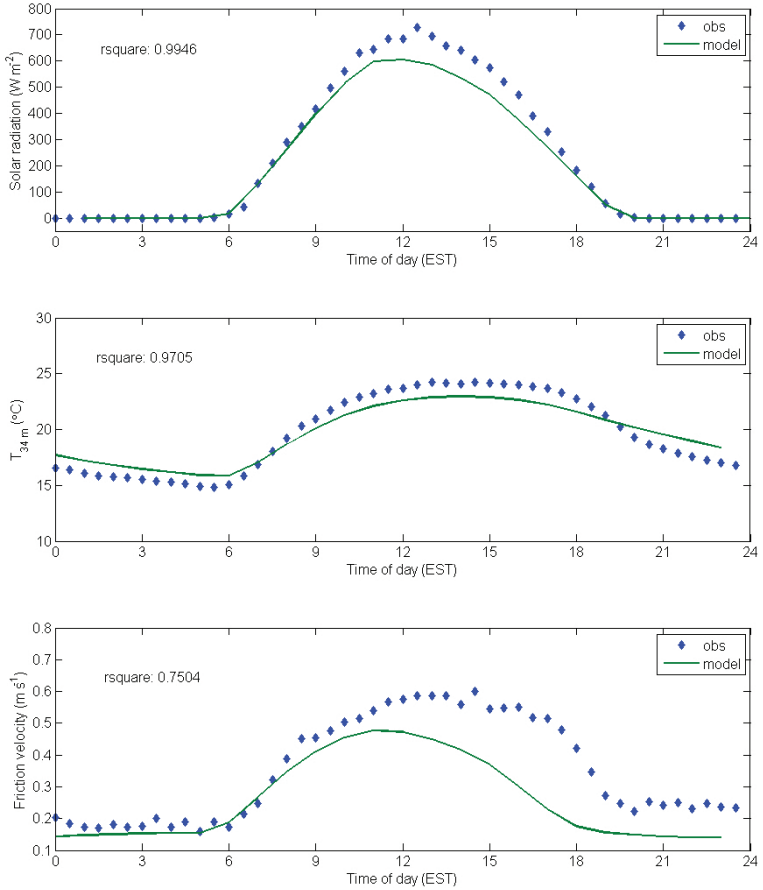

Fig. 7. Observed and modeled (SCM) diurnal variation of solar radiation, above-canopy temperature at 34 m, and above-canopy friction velocity at 46 m for August 2008 at the UMBS AmeriFlux tower. The correlation coefficient, r^2, between the observed and the modeled data is noted in each plot.

ACPD
12, 32515–32564, 2012

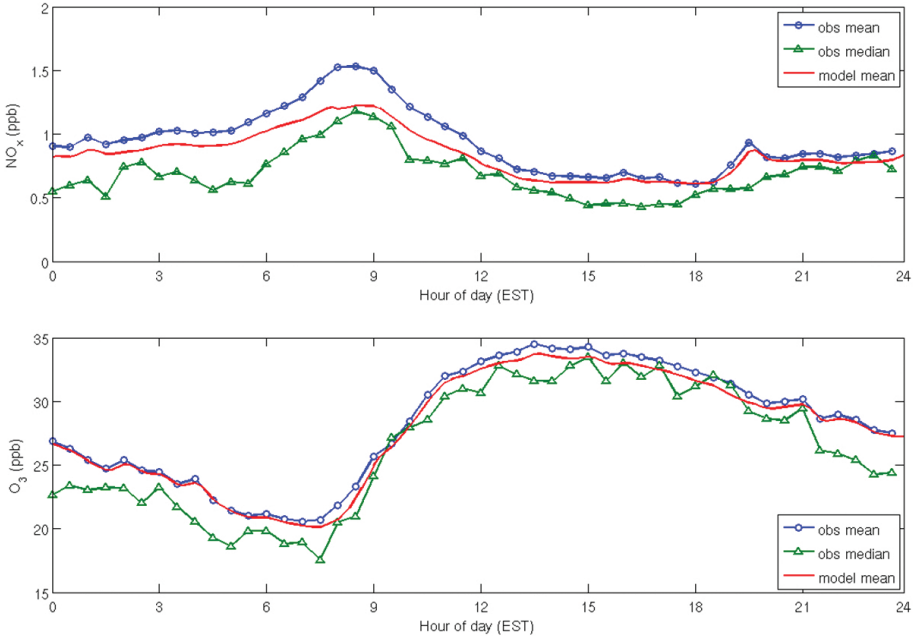

Fig. 8. Observed August mean (blue circle) and median (green triangle) diurnal cycle in NO_x and O_3 mixing ratios above the canopy at 34 m. Also shown are the simulated August mean (red line) diurnals mixing ratios.

ACPD
12, 32515–32564, 2012

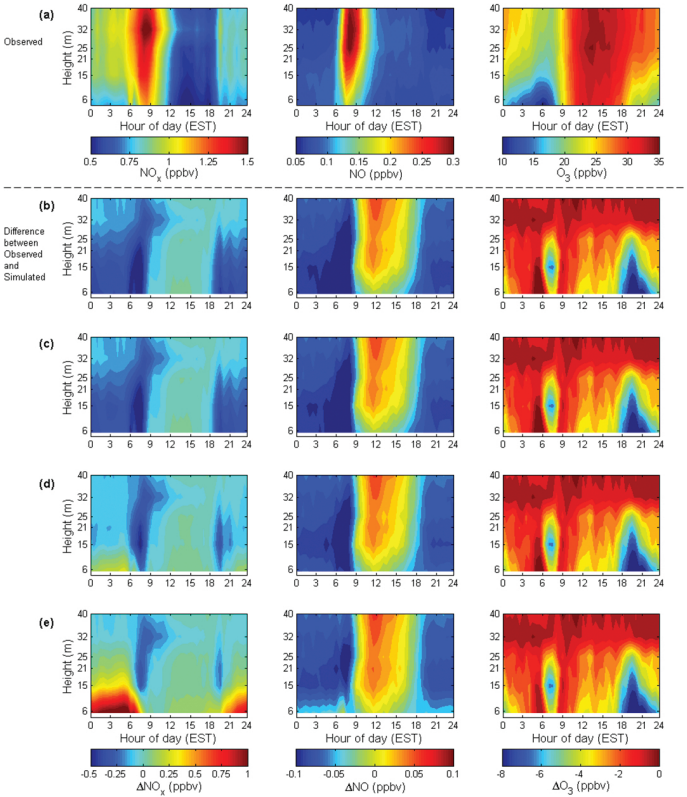

Fig. 9. (a) The observed mean diurnal mixing ratio profiles of NO_x, NO, and O_3. Plots **(b)** through **(e)** depict the difference between the observed and simulated mean (Δ = simulated – observed) diurnal cycle of the mixing ratio profiles of these gases as a function of soil NO emission for August 2008. **(b)** Case for "zero" soil emission. **(c)** Case for default soil emission (1×, 0.07 ng N m^{-2} s^{-1}; see Table 1). **(d)** Case for 10 times the default soil emission (10×). **(e)** Case for 25 times the soil emission (25×).

ACPD
12, 32515–32564, 2012

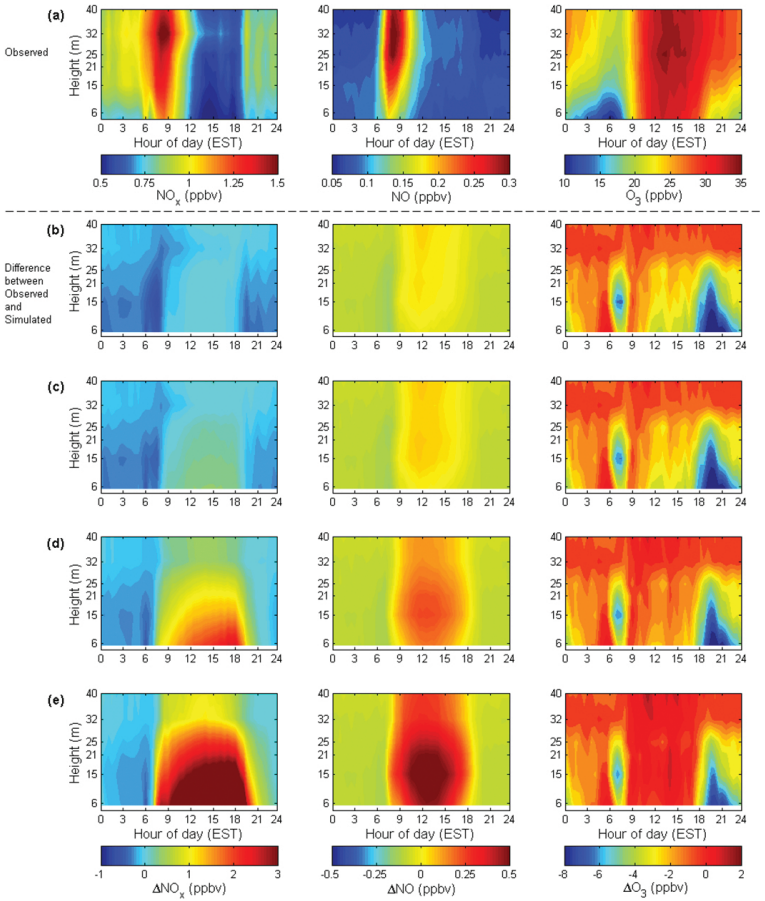

Fig. 10. Similar to Fig. 9 but for sensitivity towards foliage NO_x emission. **(a)** The observed mean diurnal mixing ratio profiles, **(b)** case for "zero" foliage emission, **(c)** 1× case, **(d)** 10× case, **(e)** 25× case.

ACPD
12, 32515–32564, 2012

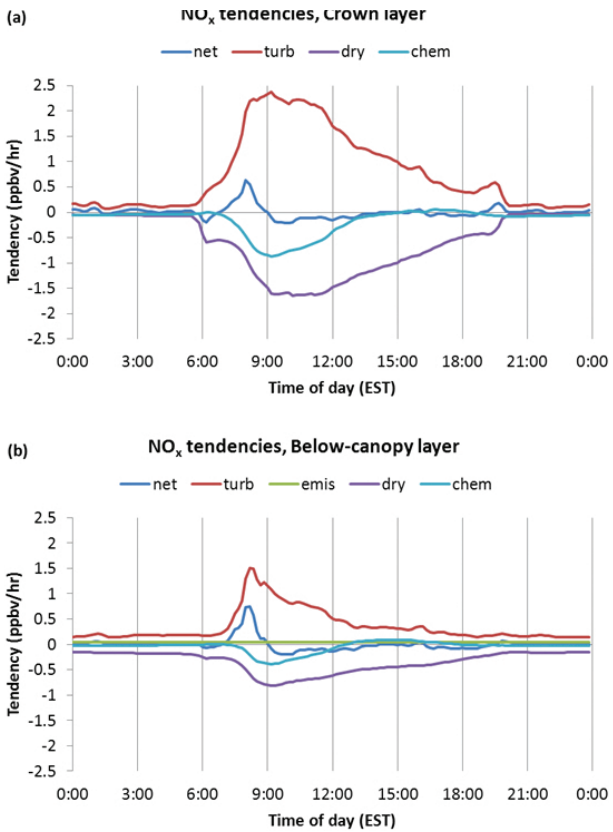

Fig. 11. Simulated August mean diurnal cycle in NO_x process tendencies (ppbv h^{-1}) of emissions (red solid line), dry deposition (green long-dashed line), chemistry (blue short-dashed line), turbulent transport (maroon dashed line), and the net tendency (black solid line) **(a)** in the crown layer and **(b)** in the understory layer.

ACPD
12, 32515–32564, 2012

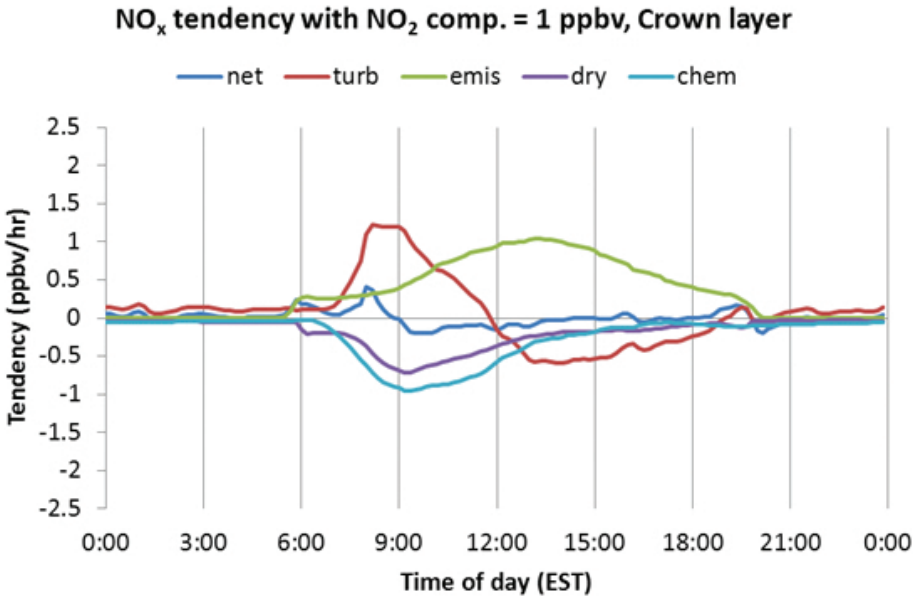

Fig. 12. Similar to Fig. 11a but showing the simulated August mean diurnal cycle in NO_x process tendencies (ppbv h^{-1}) for the crown layer for an assumed NO_2 compensation point of 1 ppbv.

ACPD
12, 32515–32564, 2012

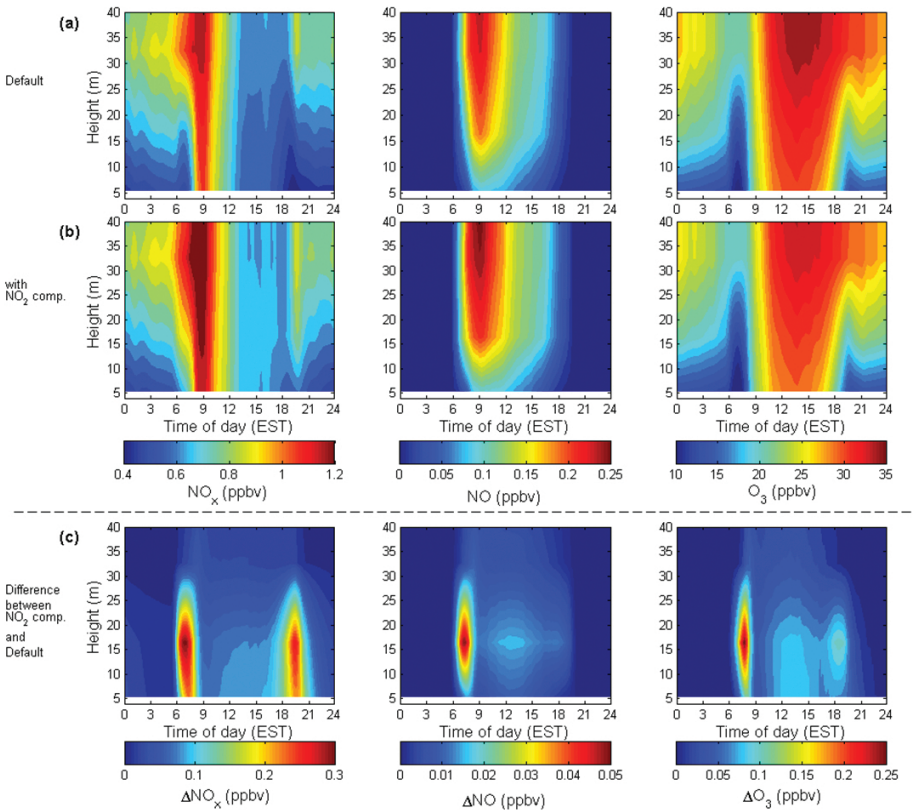

Fig. 13. Simulated August diurnal vertical profiles of NO_x, NO, and O_3 mixing ratios using **(a)** default parameters and **(b)** parameters with 1 ppbv NO_2 compensation point. **(c)** The difference between simulation considering NO_2 compensation point and the default (Δ = NO_2 compensation point simulation – default simulation).

ACPD
12, 32515–32564, 2012